

Electronic Thesis and Dissertation Repository

8-21-2020 10:30 AM

Effect of moving boundary on fluid flow

Kh Md Faisal, *The University of Western Ontario*

Supervisor: Floryan, J. M., *The University of Western Ontario*

A thesis submitted in partial fulfillment of the requirements for the Master of Engineering
Science degree in Mechanical and Materials Engineering

© Kh Md Faisal 2020

Follow this and additional works at: <https://ir.lib.uwo.ca/etd>



Part of the [Mechanical Engineering Commons](#)

Recommended Citation

Faisal, Kh Md, "Effect of moving boundary on fluid flow" (2020). *Electronic Thesis and Dissertation Repository*. 7246.

<https://ir.lib.uwo.ca/etd/7246>

This Dissertation/Thesis is brought to you for free and open access by Scholarship@Western. It has been accepted for inclusion in Electronic Thesis and Dissertation Repository by an authorized administrator of Scholarship@Western. For more information, please contact wlsadmin@uwo.ca.

Abstract

The peristaltic pumping through channels with vibrating walls has been studied. The vibrations take the form of traveling waves. The spectrally accurate algorithm used to study flow properties is based on the Fourier expansions in the flow direction, Chebyshev expansions in the transverse direction, and the immersed boundary conditions (IBC) concept to deal with the irregular form of the solution domain associated with the waves. The flow domain is immersed in a regular computational domain. The flow boundary conditions are imposed in the form of constraints. Effectiveness of peristaltic pumping is assessed by determining the variation in the flow rate created by the wall vibrations. The study includes analysis of vibrations of just one wall as well as both walls. The effects of variations of the wave wavenumber, its amplitude, and the phase speed are analyzed. The effect of the relative position of the waves on different walls is studied in the case of the two wall vibrations. The results show that the flow rate is nearly constant and marginally dependent on the wave wavenumber as long as this wavenumber is sufficiently small but rapidly increases when the wavenumber becomes larger than one. The flow rate increases proportionally to the second power of the wave amplitude and proportionally to the first power of the wave phase speed. The largest flow rate is achieved for the two-wave system when the phase difference between both waves is equal to the half of their wavelength.

Keywords

Peristaltic pumping, pumping, immersed boundary condition method, vibrating wall, spectral discretization, channel flow.

Summary for Lay Audience

The application of moving boundaries in the form of peristaltic pumping is available in many biological and engineering systems. Understanding this effect is, hence, crucial. To understand this effect, channel flow will be considered as a sample problem. The focus of this work will be on the modification of channel flow resulting from the transverse movement of the bounding walls in the form of a traveling wave. Waves can be created using properly distributed piezoelectric pistons with a relevant phase difference. Investigations will be carried out considering constant pressure gradient constraint.

This project will help to have more insight into the effect of peristaltic pumping which can be used to tailor numerous applications involving this concept to get the desired performance.

Acknowledgments

At first, I would like to express my deep gratitude towards my respected and honorable supervisor Prof. J. M. Floryan for his continuous support and unparalleled assistance. He was always there to support and bless me with his precious guidance irrespective of day and night, weekday and weekend. My work would not be finished without such support. Words are not enough to express my thankfulness towards him for his patience, motivation, enthusiasm, kindness, sympathy, generosity, and enormous knowledge. His guidance helped me a lot in all the time of research and writing of this thesis.

I am also thankful to the members of my advisory committee, Prof. R.E. Khayat, Prof. C.T. DeGroot for their encouragement and constructive comments. Also, I am grateful to Prof. L.Y. Jiang for her advice and support.

I am deeply indebted to Dr. Hadi Vafadar Moradi. It would be very difficult for me to understand research methodology without his support and guidance. I received both intellectual and mental support from him.

I am very especially thankful to Shoyon Panday Riko. He supported me in every possible way, be it in writing code in research or be it in overcoming stresses in the difficult times of my life. He went out of his way to extend his help with utmost sincerity.

I would like to thank all my colleagues Dr. Mohammad Zakir Hossain, Sahab Zandi, Sakib Shadman, Yanbei Wang, Carlos Azael Alvarez, Ly jiao, Dr. Josuel Kruppa Rogenski, Adriano Takata, Nafisha Nubayaatt Haq for their friendship and encouragement.

I also want to thank my loving and hard-working parents who sacrificed their happiness to make the best of me and my brother's life.

Finally, I would like to mention that this work has been carried out with the financial support received from the Natural Sciences and Engineering Research Council (NSERC) of Canada.

Table of Contents

Abstract	ii
Summary for Lay Audience	iii
Acknowledgments	iv
List of Figures	viii
List of Abbreviations, Symbols, and Nomenclature	x
Chapter 1	1
1 Introduction	1
1.1 Objectives	2
1.2 Motivations	2
1.3 Literature Review	2
1.3.1 Review on peristalsis with magnetohydrodynamics	3
1.3.2 Review on peristalsis through porous media	4
1.3.3 Review on peristaltic flow of nanofluids	5
1.3.4 Review on peristaltic flow of couple-stress fluid	5
1.3.5 Review on peristaltic flow of non-Newtonian fluids	6
1.3.6 Review on Peristaltic pumping in Esophagus	8
1.4 Methodology	9
1.5 Outline of this work	12
Chapter 2	13
2 Problem Formulation	13
2.1 The geometry of flow domain	13
2.2 Governing equations, boundary conditions and equation of constraint	14
2.3 Determination of stresses and forces	15
2.4 Introducing Galileo transformation	18

Chapter 3.....	20
3 Numerical Solution	20
3.1 Introducing function ψ	20
3.1.1 Governing equation after introducing function ψ	20
3.1.2 Boundary conditions after introducing function ψ and equation of constraint.....	20
3.1.3 Function ψ along the boundaries	21
3.2 Discretization Method.....	21
3.2.1 Discretization of governing equations	22
3.2.2 Discretization of boundary conditions and pressure gradient constraint ..	24
3.3 Solution Process.....	29
3.3.1 Iterative solution process	29
3.3.2 Method of updating nonlinear terms.....	30
3.4 Post-Processing.....	32
Evaluation of stresses and forces along the boundaries.....	32
Chapter 4.....	39
4 Results and Discussion.....	39
4.1 Effect of the wave wavenumber	39
4.2 Effect of variations of the wave amplitude	46
4.3 Effect of variations of the wave phase speed.....	47
4.4 Effect of the phase difference	48
Chapter 5.....	50
5 Conclusions and Recommendations	50
5.1 Conclusions.....	50
5.2 Recommendations for future work	52
References.....	52

Appendices.....	60
Appendix A: Evaluation of Fourier Expansion of Chebyshev Polynomials and their derivatives	60
Evaluation of Fourier Expansion of Chebyshev Polynomials	60
Evaluation of Fourier Expansion of first derivative of Chebyshev Polynomials .	64
Appendix B: Evaluation of Innerproducts of Chebyshev polynomials and their derivatives	66
Curriculum Vitae	70

List of Figures

Figure 1	1
Figure 2: Channel with moving boundary	13
Figure 4.1 (a) Variation of the flow rate Q as a function of the wavenumber for different wave phase speeds c . Dashed and solid lines correspond to the wave amplitudes $A=0.05$ and 0.01 respectively. Dotted lines represent asymptotes. (b) Variations of the force components (the x -component of the shear force $F_{Xv,L}$ (dotted line), the x -component of the pressure force $F_{Xp,L}$ (dashed line) acting on the fluid at the lower wall and the x -component of the shear force $F_{Xv,U}$ (dash-dotted line) acting on the fluid at the upper wall) as functions of the wavenumber α . The variations of the flow rate Q are represented by solid lines. These computations are done for the amplitude $A = 0.01$ and the wave phase speed $c = 5$	40
Figure 4.2 (a) Sketch of the lower wall with the small wavenumber waves; (b) Sketch of the lower wall with the large wavenumber waves.....	41
Figure 4.3 (a) Distribution of the x -component of the pressure force acting on the fluid at the lower wall over one wavelength, (b) Distribution of the x -component of the shear force acting on the fluid at the lower wall over one wavelength, (c) Distribution of the x -component of the shear force acting on the fluid at the upper wall over one wavelength. In all plots, solid lines represent forces and the dashed lines represent wave shape. All these plots correspond to the wave amplitude $A = 0.01$ and the wave phase speed $c = 5$	41
Figure 4.4: u -velocity profiles at selected locations. At each location, the variation of the u -velocity profile is shown for selected wavenumbers. Computations are carried out for the amplitude $A = 0.01$ and the wave phase speed $c = 5$	44
Figure 4.5 u -velocity profiles for selected wavenumbers. At each wavenumber, the variation of the u -velocity profile is shown at four different locations. Computations are carried out for the wave amplitude $A = 0.01$ and the wave phase speed $c = 5$	45

Figure 4.6 Plots of velocity fields. (a) to (f) correspond to $\alpha = 0.1, 2, 5, 7, 10, 45$, respectively, for the wave phase speed $c = 5$ and the wave amplitude $A = 0.01$. Flow zones with fluid moving in the opposite direction are identified using shading. 46

Figure 4.7 Plots of variations of the flow rate Q as a function of the wave amplitude A for selected wave phase speeds $c = 1, 5, 10$. Dashed lines correspond to the wavenumber $\alpha = 0.1$ and solid lines correspond to the wavenumber $\alpha = 10$ 47

Figure 4.8 Plots of variations of the flow rate Q as a function of the wave phase speed c for selected wavenumbers ($\alpha = 0.1, 2, 5, 7, 10$)..... 48

Figure 4.9 Plots of variation of the flow rate Q as a function of the phase difference between the waves at the upper and lower walls for the phase speed $c = 5$ and the amplitude $A = 0.01$ for selected wavenumbers. Dashed lines indicate corresponding cases with one wall vibration. 49

List of Abbreviations, Symbols, and Nomenclature

Abbreviations

IBC	Immersed boundary condition
RF	Relaxation factor
FFT	Fast Fourier transform
IB	Immersed boundary
DT	Domain Transformation
DP	Domain Perturbation

Symbols and Nomenclature used in Chapter 2

h	Half of the average channel height
$\pm\infty$	Positive and negative infinite
(t, X, Y)	Time-dependent physical coordinate system
$Y_U(t, X)$	Time-dependent geometry of the upper wall of the channel
$Y_L(t, X)$	Time-dependent geometry of the lower wall of the channel
B_U	Wave amplitude of the upper wall wave
B_L	Wave amplitude of the lower wall wave
H_U	The function describing the upper wall waveform
H_L	The function describing the lower wall waveform
c	Wave phase speed
t	Time

N_A	Number of Fourier modes required to describe wave shapes
(n)	Fourier mode (as superscript)
α	Wavenumber
(u, v)	Velocity vector with components in the (X, Y) -directions scaled with $U_v = v/h$ as the velocity scale
p	Pressure scaled with ρU_v^2 as the pressure scale
t	Time-scaled with h/U_v
ν	Kinematic viscosity
ρ	Density
$\left. \frac{\partial p}{\partial x} \right _{mean}$	Mean pressure gradient
$Q _{mean}$	Mean flow rate
$\vec{\sigma}_L$	The stress vector acting on the lower wall wave
$\sigma_{X,L} \quad \sigma_{Y,L}$	The x -and y -component of the stress vector acting on the lower wall wave
\vec{n}_L	The normal unit vector acting on the lower wall wave
$n_{X,L}$	The x -component of the normal unit vector on the lower wall wave
$n_{Y,L}$	The y -component of the normal unit vector on the lower wall wave
$\sigma_{Xv,L}$	The x -component of viscous stress acting on the lower wall wave
$\sigma_{Xp,L}$	The x -component of normal stress generated due to pressure acting on the lower wall wave
$\sigma_{Yv,L}$	The y -component of viscous stress acting on the lower wall wave

$\sigma_{Yp,L}$	The y -component of normal stress generated due to pressure acting on the lower wall wave
$\sigma_{n,L}$	The normal stress vector acting on the lower wall wave
$\sigma_{t,L}$	The tangential stress vector acting on the lower wall wave
$\sigma_{nv,L}$	The normal component of viscous stress acting on the lower wall wave
$\sigma_{np,L}$	The normal component of stress generated due to pressure acting on the lower wall wave
$F_{X,L}$	The x -component of total force acting on the lower wall wave
$F_{Y,L}$	The y -component of total force acting on the lower wall wave
λ	Wavelength
X_0	A convenient reference point
$F_{Xv,L}$	The x -component of viscous force acting on the lower wall wave
$F_{Xp,L}$	The x -component of pressure force acting on the lower wall wave
$F_{Yv,L}$	The y -component of viscous force acting on the lower wall wave
$F_{Yp,L}$	The y -component of pressure force acting on the lower wall wave
$\vec{\sigma}_U$	The stress vector acting on the upper wall wave
$\sigma_{X,U}$ $\sigma_{Y,U}$	The x - and y -component of the stress vector acting on the upper wall wave
\vec{n}_U	The normal unit vector acting on the upper wall wave
$n_{X,U}$	The x -component of the normal unit vector on the upper wall wave

$n_{Y,U}$	The y -component of the normal unit vector on the upper wall wave
$\sigma_{X,U}$	The x -component of total normal stress acting on the upper wall wave
$\sigma_{Xv,U}$	The x -component of viscous stress acting on the upper wall wave
$\sigma_{Xp,U}$	The x -component of normal stress generated due to pressure acting on the upper wall wave
$\sigma_{Y,U}$	The y -component of total normal stress acting on the upper wall wave
$\sigma_{Yv,U}$	The y -component of viscous stress acting on the upper wall wave
$\sigma_{Yp,U}$	The y -component of normal stress generated due to pressure acting on the upper wall wave
$\sigma_{n,U}$	Total normal stress vector acting on the upper wall wave
$\sigma_{t,U}$	The tangential stress vector acting on the upper wall wave
$\sigma_{nv,U}$	The normal component of viscous stress acting on the upper wall wave
$\sigma_{np,U}$	The normal component of stress generated due to pressure acting on the upper wall wave
$\sigma_{t,U}$	The tangential component of stress acting on the upper wall wave
$F_{X,U}$	The x -component of total force acting on the upper wall wave
$F_{Xv,U}$	The x -component of viscous force acting on the upper wall wave
$F_{Xp,U}$	The x -component of pressure force acting on the upper wall wave
$F_{Y,U}$	The y -component of total force acting on the upper wall wave

$F_{Yv,U}$	The y -component of viscous force acting on the upper wall wave
$F_{Yp,U}$	The y -component of pressure force acting on the upper wall wave
H_{tot}	The total force acting on the fluid at both walls per unit length of the channel
$H_{tot,X}$	The x -component of total force acting on the fluid at both walls per unit length of the channel
$H_{tot,Y}$	The y -component of total force acting on the fluid at both walls per unit length of the channel
(x, y)	Coordinate system after Galileo transformation
y_U, y_L	Shapes of the waves at the upper and the lower walls in the transformed coordinate system

Symbols and Nomenclature used in Chapter 3

N_{uv}	Nonlinear velocity terms
(x, \hat{y})	Computational Coordinate system
y_t, y_b	Locations of extremities of the upper and lower walls respectively
Γ	Constant associated with the coordinate transformation for the IBC method
$\widehat{u}\widehat{u}, \widehat{u}\widehat{v}, \widehat{v}\widehat{v}$	Velocity products in the physical space
\hat{y}_U, \hat{y}_L	Upper and lower wall wave shapes in the computational coordinate system
$A_U^{(n)}, A_L^{(n)}$	Coefficient of Fourier expansions that express the wave geometries at the upper and lower walls in the computational domain

$\widehat{uu}^{(m)}, \widehat{uv}^{(m)}, \widehat{vv}^{(m)}$	Modal functions of velocity products in the physical space ($\widehat{uu}, \widehat{uv}, \widehat{vv}$)
$u^{(m)}, v^{(m)}, p^{(m)}$	Modal functions of u, v, p
N_M	Number of Fourier modes
N_T	Order of Chebyshev polynomials used for discretization of the modal functions in the transverse direction in computational coordinate
T_k	k -th Chebyshev polynomials of the first kind
D	Derivative with respect to the transverse direction
$G\psi_k^{(m)}$	Coefficient of Chebyshev expansion of $\psi^{(m)}$
$G\widehat{uu}_k^{(m)}, G\widehat{uv}_k^{(m)}, G\widehat{vv}_k^{(m)}$	Coefficient of Chebyshev expansion of $\widehat{uu}^{(m)}, \widehat{uv}^{(m)}, \widehat{vv}^{(m)}$
$Gu_k^{(m)}, Gv_k^{(m)}, GP_k^{(m)}$	Coefficient of Chebyshev expansion of $u^{(m)}, v^{(m)}, p^{(m)}$
i	Imaginary unit
$\langle T_j, D^n T_k \rangle$	The inner product of a Chebyshev polynomial of j -th order and its n -th derivative
$\langle T_j, T_k \rangle$	The inner product of two Chebyshev polynomials of j -th and k -th order
$\langle f, g \rangle$	The inner product of two functions
$(d_U)_k^{(m)}, (d_L)_k^{(m)}$	Coefficients of the Fourier expansions for the first derivative of the Chebyshev polynomials evaluated at the upper and lower wall wave
$(w_U)_k^{(m)}, (w_L)_k^{(m)}$	Coefficients of the Fourier expansions of the Chebyshev polynomials evaluated at the upper and lower wall wave

N_f	Number of Fourier modes in the Fourier expansions that express the wave geometries in the computational domain
N_s	Number of Fourier modes used to describe the Chebyshev Polynomials and their derivatives evaluated at the upper and lower wall waves

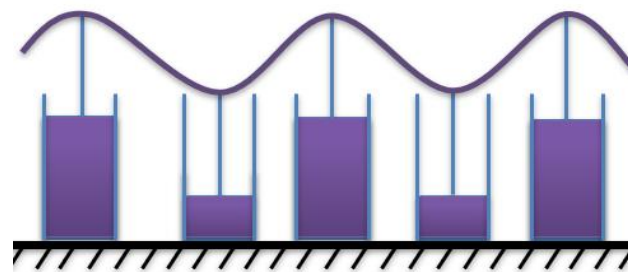
Symbols and Nomenclature used in Chapter 4

A	Wave amplitude
Ω	The phase difference between the waves at the upper and lower wall

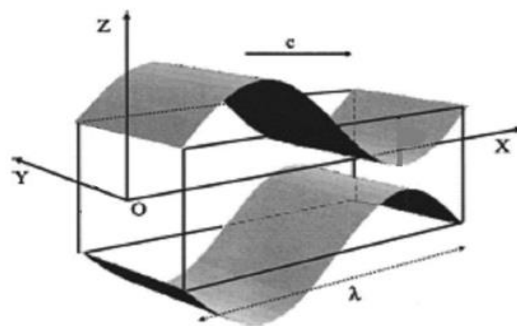
Chapter 1

1 Introduction

The applications of moving boundaries in the form of peristaltic pumping are available in many biological and engineering systems. Understanding the effect of peristaltic pumping is, hence, crucial. To understand this effect, channel flow is considered as a sample problem. The focus of this work is on the modification of channel flow resulting from the transverse movement of the bounding walls in the form of a traveling wave (as shown in Fig. 1). Waves can be created using properly distributed piezoelectric pistons (as shown in Fig. 1) with a relevant phase difference.



Moving boundary



in the form of traveling-waves

Figure 1

1.1 Objectives

The main aim of this work is to analyze the effect of moving boundaries on fluid flow in the form of peristaltic pumping. To understand the effect, flow through a channel with moving boundaries is taken into consideration. The physical mechanism activated by the moving boundary and responsible for variation in the flow response is to be investigated. This analysis is conducted under the consideration of fixed pressure gradient constraint.

1.2 Motivations

Application of this work can be found in many applications ranging from biological, medical to bio-medical and mechanical engineering. For example: in the biological system it's the application can be found in urine transportation from the kidney to bladder, food transport through the gullet. In mechanical engineering, applications can be found in peristaltic pumps. Hence, understanding this effect in full is crucial. While the literature on the subject is quite voluminous, fundamental aspects of the flow response to the presence of boundary movements have yet to be explained.

1.3 Literature Review

Peristalsis is a mechanism either to mix contents in a container or propel the contents through a duct. Application of this is widely found in engineering, medical and biomedical applications. In the case of biological applications, examples are mixing of contents inside bile duct, ureter, glandular duct, etc. Peristaltic transport is assumed to have a solution for many of the engineering and biomedical problems.

When fluids are being transmitted only through expansion and contraction of muscles then this is referred to as peristaltic pumping whereas the process is named as peristalsis. This

term was first coined by Bayliss and Starling (1902). A nice example of peristalsis can be our eating process where the food bolus moves through the esophagus after we swallow it. This movement takes place through the expansion and contraction of smooth muscles. Muscles that squeeze behind the food bolus, prevent it from going back. This way contractions take place like unidirectional waves that facilitate the food to reach the stomach. This is a unidirectional process as the food goes from mouth to the stomach.

Following is an overview of the existing literature on peristalsis. It shows research conducted from various perspectives. To present the review systematically, it is divided into several subsections as presented below:

1.3.1 Review on peristalsis with magnetohydrodynamics

Magnetohydrodynamic effects facilitate a form of control mechanism in a fluid flow which can be observed in the case of magnetic peristaltic pumps and other biomagnetic pumps. A better alternative to micro-pumps was proposed by Kim (2006). In his developed micropump, magnetic fluids were driven through a concentric channel by dint of magnetic force. It was claimed to be more durable and reliable than the existing micro-pumps. Several variants of the magnetohydrodynamic peristaltic pump were developed by some other researchers like Neto (2011), Al-Halhouli (2010), etc. In the field of industrial fluid dynamics, an important role is played by flow field and boundary conditions. Endoscopy can be considered as an example of that which is employed to inspect the interior of any organ. Contributions found in this stream of research are due to Abd elnaby and Misiery 2002, Abd elnaby 2004, Hayat 2006, Khan, Sohail, Ayesha, and Rashid 2015, Tripathi 2011a, Tripathi 2011b, Tripathi 2011c, Tripathi 2012d and Tripathi 2012e. These studies were on the peristaltic flow of various types of fluids (Newtonian and non-Newtonian)

between two concentric tubes. Theoretical researches were conducted on peristaltic magnetohydrodynamic flows. A study on a couple of stress fluid was conducted by Tripathi and Beg (2013). Peristalsis with magnetized nanofluid was studied by Kothandapani and Prakash (2014, 2015). The combined effect of heat transfer and magnetic induction was studied by Akbar (2015). A numerical analysis of the peristaltic flow through a circular tube was conducted by Tripathy (2011c). Studies on various pros and cons of magnetohydrodynamic peristaltic pumping are also available (Kumari and Radhakrishnamacharya (2012) and Ramesh and Devakar (2015)). Moreover, studies on the same topic with various formulations (e.g., consideration of Lorentz force, magnetic nanofluids, heat transfer, etc.) are also prevailing in the existing literature (Ellahi 2015b, Rashidi 2015, Ellahi 2015a, Sheikholeslami and Ellahi 2015).

1.3.2 Review on peristalsis through porous media

Many mathematical studies were conducted on peristalsis in porous media focusing on the digestive system. A flow model using viscous Newtonian fluid was proposed by El Shehawey (2000). Perturbation solutions were obtained for pressure gradient and stream function using this model. The analytical solution was developed by Hayat (2007) for the cases which involve a small-amplitude ratio in the peristaltic flow of viscoelastic fluids. Perturbation solution for the cases of peristaltic pumping which involves heat transfer was developed by Vajravelu (2007). Investigation of Darcy number effects in peristaltic flow and heat transfer in a porous medium was accomplished by Vasudev (2011). A generalized Darcy formulation was proposed by Tripathi and Bég (2012a) for peristalsis in porous media employing Maxwell's viscoelastic model. Investigation of diffusion in blood flow in non-Darcy porous media was conducted by Bég (2012).

1.3.3 Review on peristaltic flow of nanofluids

Nanotechnology drew great attention in the past few years for the sake of the development of medical devices on a smaller scale. The discussion on nano-fluid mechanics was pioneered by Chol (1995), focusing on the modification of micro-fluids through employing specially designed nanoparticles. It had such an impact on biomedical engineering that several journals (Journal of Nanofluids [Prasad 2015], ASME Journal of Nanotechnology in Engineering Medicine [Lu 2011]) were initiated in this stream of research. Several studies in this stream of research are - peristalsis of nanofluid through a curved channel by Hayat and Ahmed (2019), peristaltic pumping of Nanofluids in the presence of magnetohydrodynamics and thermal radiation by Prakash and Siva (2019), hydrodynamic peristalsis of Nanofluids by Hayat (2017), the endoscopic effect on the peristaltic flow of Nanofluid by Khaled (2014), an analytical solution of the peristaltic flow of Nanofluid developed by Ebaid (2013), application of peristaltic flow of Nanofluids in drug delivery system by Tripathy and Beg (2014), peristaltic pumping of Nanofluid through a tapered channel by Prakash and Tripathy (2019), etc. Mathematical studies focusing on the peristaltic flow-through channel were conducted by Akbar and Nadeem (2012), Mustafa (2012), Akbar (2012), Aly and Ebaid (2014).

1.3.4 Review on peristaltic flow of couple-stress fluid

It is a variant of non-Newtonian fluid. The peristaltic flow of this type of fluid through a channel under an oscillatory flux was investigated by Kumar (2010). The peristaltic flow of couple stress fluid under the influence of the magnetic field in an asymmetric channel was investigated by Nadeem (2011). Before that, a similar type of investigation was conducted by Nasir and Hayat (2007). The magnetohydrodynamic peristaltic flow of

couple stress fluids with heat and mass transfer was investigated by Nabil, Samy, Hasan, and Elogail (2012). The magnetohydrodynamic peristaltic flow of couple stress fluids with slip effect was investigated by Lika, Ahmed, and Liqaa (2014). A similar investigation by adding the effect of the magnetic field was conducted by Swarnalathamma and Krishna (2016). Effect of peristaltic flow of couple stress fluid in a channel at low Reynolds number was investigated by Kumar (2016). A study on the peristaltic flow of couple stress fluid through a uniform porous medium was conducted by Alsaedi, Nasir, and Tripathy (2014) whereas the peristaltic flow of couple stress fluid both in uniform and a non-uniform channel was studied by Mekheimer (2002). The exact solution for the peristaltic flow of couple stress fluid was worked out by Hina, Mustafa, and Hayat (2015). Peristaltic flow with heat and mass transfer tailoring it to an application of biomedicine was also investigated by them (2015). A blood flow model was proposed by Kumar (2015) where the effect of couple stress fluid on magnetohydrodynamic peristaltic flow with a porous medium through an inclined channel at the presence of slip effect was investigated by him. The magnetohydrodynamic peristaltic flow of a couple stressed fluid through a porous medium with long-wavelength approximation was studied by Mohanakrishnan and Siva (2015). Thermal properties of couple stress fluid in an asymmetric channel with peristalsis were studied by Elmaboud, Mekheimer, and Abdellateef (2013). Hall effects of the same type of fluid in a vertical asymmetric channel was studied by Kumar, Kavitha, and Saravana (2017).

1.3.5 Review on peristaltic flow of non-Newtonian fluids

Several studies were conducted on the peristaltic flow of various kinds of non-Newtonian fluids. The non-Newtonian effects of the peristaltic flow of a Maxwell fluid were

investigated by Tsiklauri and Beresnev (2001). The slip effect on a non-Newtonian Maxwellian fluid in the case of peristaltic flow was studied by El-Shehawey, El-Dabe, and Eldesoky (2006). The magnetohydrodynamic peristaltic flow of non-Newtonian fluid through a circular cylindrical tube was investigated by Eldabe, Nabil, and Ghaly, A.Y. and Sayed, Haneen (2007). The peristaltic flow of a non-Newtonian fluid under the influence of the magnetic field in a planar channel was investigated by Hayat, Tasawar, and Khan, M. and Siddiqui, Abdul, and Asghar, Saleem (2007). The peristaltic flow of non-Newtonian fluid in a curved channel was studied by Nasir and Sajid (2010). A similar numerical study was conducted by Kalantari, Sadeghy, and Sadeqi (2013). Non-Newtonian characteristics of the peristaltic flow of blood in micro-vessels were studied by Maiti and Misra, (2011). The compressibility effects on peristaltic flow through an annulus in the case of non-Newtonian Maxwell fluid were investigated by Mekheimer and Abdel-Wahab, Hina, Sadia (2013). The peristaltic flow of Pseudoplastic fluid in a curved channel was explored by Mustafa, Meraj, Hayat, Tasawar, and Alsaedi (2013). The effect of wall properties on the peristaltic flow of a non-Newtonian Fluid was worked out by Javed, Maryam, Hayat, Tasawar, and Alsaedi (2014). An analysis of the convective heat transfer of the peristaltic flow of power-law fluid in a channel was conducted by Hayat, Tasawar, Yasmin, Humaira, and Alsaedi (2014). A mathematical study of non-Newtonian fluid through composite stenosis in the case of arterial blood flow was conducted by Ellahi and Rahmat (2014) along with their group. An exact solution of the peristaltic flow of non-Newtonian fluid was proposed by Singh (2016). The peristaltic flow of non-Newtonian fluid through a nonuniform tube was also analyzed by him along with Medhavi, Gupta, and Bhatt (2017). Recently, modeling and simulation of the peristaltic flow of Newtonian

and non-Newtonian fluids with application to the human body were accomplished by Samer (2017). Research on the peristaltic flow of an Ellis fluid in an inclined uniform tube was conducted by Kumar, Thanesh, Kavitha, and Saravana (2018). The peristaltic flow of non-Newtonian Maxwell fluid through a heated non-uniform tube was investigated by Vaidya and Choudhari (2019) along with their group.

1.3.6 Review on Peristaltic pumping in Esophagus

The peristaltic pressure profiles of the human esophagus were studied by Gernhardt and Castell (2000). The effect of gravity on oesophageal peristalsis in the human body was investigated by Allen and Zamani (2003). An artificial Esophagus with Peristaltic Movement was designed by Makoto and Sekine (2005) along with their group. Property evaluation of an artificial esophagus with peristaltic motion was done by Miki and Hiroyuki (2010) along with their group. A peristaltic pump based on bowl peristalsis was developed by Suzuki and Nakamura (2010). A study on the shape optimization of peristaltic pumping was conducted by Shawn and Shelley (2010). A mathematical model on peristaltic flow through the esophagus was proposed by Toklu (2011). A model for the movement of food through the esophagus was designed by Misra and Maiti (2011). A peristaltic actuator for esophageal swallowing was developed by Dirven and Steven (2014) along with their group. The sinusoidal peristaltic waves for mimicry of esophageal swallowing were analyzed by Dirven, Xu, Peter, Cheng, and Leo (2014). A study on the characterization of the biomimetic peristaltic pumping system was conducted by Esser and Krüger (2019) along with their group.

1.4 Methodology

Moving boundaries can be considered as dynamically evolving grooves or boundary irregularities. There are many engineering problems pertinent to the fluid flow which involves the effect of boundary irregularities on the flow. Flow problems where these boundary irregularities are stationary are referred to as "fixed boundary problems". When these irregularities dynamically evolve, then the boundary can be considered as a moving boundary.

How this moving boundary is going to affect the flow response? This is to be investigated in the proposed research. To achieve this research objective, it is essential to compute the flow modifications that occurred to mean flow due to the moving boundary. This is done by solving steady Navier-Stokes equations. It necessitates an efficient and accurate algorithm that allows simple modeling of moving boundaries. In the following section, a review of the available algorithm is presented from which the most suitable one is selected.

Most of the available algorithms for solving flow problems with boundary irregularities (stationary or dynamically evolving) involves the generation of boundary conforming grids based on finite-volume, finite element schemes (Croce 2005; Yoon 2006).

These methods use low order discretization schemes which results in lower spatial accuracy. Using these methods, one needs to use a very fine grid or need to apply higher-order schemes. Both have limitations. The use of a very fine grid is associated with unreasonable computational cost whereas the application of higher-order schemes is associated with the increased effort in formulations, complexity in programming, and grid

construction (Jiang 2005). Again, efficiencies of all the methods drop when it is required to investigate a good number of geometries.

Other methods that are based upon the numerical or analytical mapping of the physical domain are Domain Transformation (DT), Domain Perturbation (DP), and Immersed Boundary (IB) method.

In the DT method, physical boundary irregularities are analytically mapped into a regular computational domain. High spatial accuracy is achievable by combining the DT method with the spectral discretization of the transformed spatial coordinate (Husain and Floryan 2007, Angelis 1997). However, this comes with the complication in the transformed field equation which leads to an increase in computational cost for generating coefficient matrix. Hence, it is advisable to use spectral implementation of the DT method in case flow problems with high irregularities (on boundaries) only.

The domain perturbation (DP) method uses the regular computational domain. This method transfers the boundary conditions to a mean location instead of enforcing them to the edges of the physical domain (Tsangaris 1986). But, the applicability of this method is confined to irregularities with a very small amplitude (Cabal 2002).

Immersed boundary (IB) method uses regular computational domains like DT and DP method but the boundaries of the computational domain extend beyond the boundaries of the physical domain. IB methods do not require to generate a body-conforming grid. This has made this method computationally efficient. There are a good number of variants of the immersed boundary method developed by various researchers from time to time (Mittal 2005, Peskin 2002). Most of the IB methods have low spatial accuracy due to their

dependence on low order finite difference, finite volume, or finite element techniques (Mittal 2005).

From the discussion presented above, it is observed that a common limitation of the methods is the dependence of them on low-order discretization techniques which leads to low spatial accuracy. A promising method to get out of this limitation is the spectral method as it can provide the highest accuracy in case of spatial discretization.

A novel algorithm that takes advantage of the efficiency of the immersed boundary method and combines it to the highest accuracy of spectral discretization, was developed by Szumbariski and Floryan (1999). It is called the "Immersed Boundary Conditions (IBC)" method. This method is used for this research project.

According to the IBC method, assuming the flow to be periodic, the field equation is discretized using Fourier expansion in the stream-wise direction which leads the governing partial differential equation into a set of ordinary differential equations. In the direction normal to the wall, discretization is done using Chebyshev polynomials which results in a set of algebraic equations of unknown coefficients of Chebyshev polynomial (Canuto 1987).

In this algorithm, moving boundaries are considered to be periodic and modeled in terms of Fourier expansion. In the IBC method, the boundary value problem turns into an internal value problem as the discretized boundary conditions are placed as internal constraints in the algorithm. So, for the proposed research IBC method is going to be used for the reasons as explained above.

1.5 Outline of this work

The objective of this work is to explain mechanics of fluid response to boundary movements. The interest is in a special class of movements, i.e. boundary movements in the form of travelling waves which generate peristaltic pumping effect. Detailed explanation of the mechanics of this movement, description of the process leading to pumping as well as its basic parametrization will be discussed. The presentation is organized as follows. Chapter 1 describes the objectives, motivations of this work. It also provides a brief literature review on related topics. This chapter concludes with the description of the available methodologies and explains out of these methodologies, why the current one is used for this work. Chapter 2 discusses the problem formulation. Chapter 3 illustrates the numerical solution method. Chapter 4 presents the outcome of the analysis. Chapter 5 gives a summary of conclusions and gives directions for future work.

Chapter 2

2 Problem Formulation

This chapter describes the problem formulation.

2.1 The geometry of flow domain

A two-dimensional slot formed by two parallel plates placed at a distance $2h$ apart as shown in Fig.2 and extending to $\pm\infty$ in the X -direction is considered. Both plates are subjected to vibrations in the form of traveling waves with known shapes.

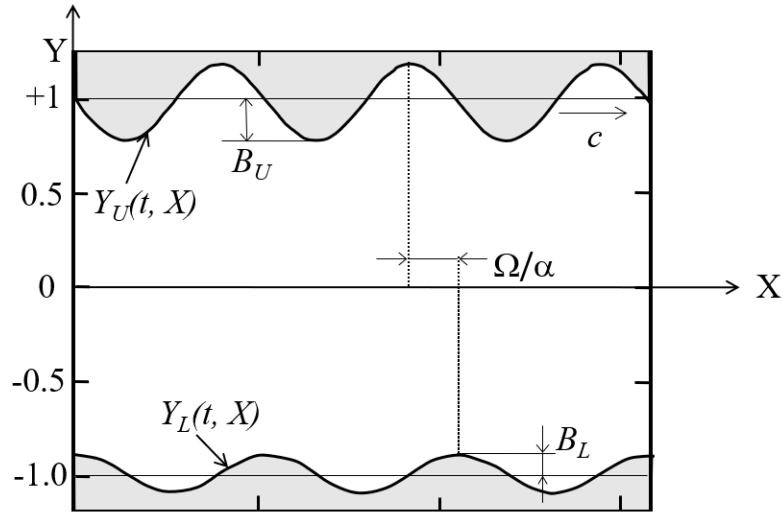


Figure 2: Channel with moving boundary

The resulting time-dependent slot geometry is described as

$$Y_U(t, X) = 1 + B_U H_U(X - ct) = 1 + B_U \sum_{n=-N_A}^{n=N_A} H_U^{(n)} e^{in\alpha(X-ct)}, \quad (2.1a)$$

$$Y_L(t, X) = -1 + B_L H_L(X - ct) = -1 + B_L \sum_{n=-N_A}^{n=N_A} H_L^{(n)} e^{in\alpha(X-ct)} \quad (2.1b)$$

where subscripts U, L refer to the upper and lower walls, H_U and H_L are the known functions describing waveforms satisfying the following conditions

$$-\frac{1}{2} \leq H_U(X - ct) \leq \frac{1}{2}, \quad -\frac{1}{2} \leq H_L(X - ct) \leq \frac{1}{2}, \quad (2.1c)$$

B_U and B_L are the wave amplitudes, N_A denotes the number of Fourier modes required to describe wave shapes, c and α denote the wave phase speed and wavenumber, respectively, $H_U^{(n)} = H_U^{(-n)*}$ and $H_L^{(n)} = H_L^{(-n)*}$ are the real conditions with $*$ denoting the complex conjugates and all quantities have been scaled with h as the length scale.

2.2 Governing equations, boundary conditions and equation of constraint

The character of fluid movement induced by surface waves is described by the Navier-Stokes and continuity equation of the form

$$\frac{\partial u}{\partial t} + u \frac{\partial u}{\partial X} + v \frac{\partial u}{\partial Y} = -\frac{\partial p}{\partial X} + \frac{\partial^2 u}{\partial X^2} + \frac{\partial^2 u}{\partial Y^2}, \quad (2.2a)$$

$$\frac{\partial v}{\partial t} + u \frac{\partial v}{\partial X} + v \frac{\partial v}{\partial Y} = -\frac{\partial p}{\partial Y} + \frac{\partial^2 v}{\partial X^2} + \frac{\partial^2 v}{\partial Y^2}, \quad (2.2b)$$

$$\frac{\partial u}{\partial X} + \frac{\partial v}{\partial Y} = 0, \quad (2.2c)$$

where (u, v) denotes velocity vector with components in the (X, Y) -directions scaled with $U_v = \nu/h$ as the velocity scale, p denotes pressure scaled with ρU_v^2 as the pressure scale and t stand for time scaled with h/U_v as the time scale. In the above, ν denotes kinematic viscosity, and ρ stands for density. The appropriate boundary conditions are

$$Y = Y_U(X, t): \quad u = 0, \quad v = \frac{\partial Y_U}{\partial t}, \quad (2.2d)$$

$$Y = Y_L(X, t): \quad u = 0, \quad v = \frac{\partial Y_L}{\partial t}. \quad (2.2e)$$

Fluid motion, if any, including the net flow rate in the x -direction, can be induced solely by the wall vibrations and this necessitates the imposition of a constraint which eliminates any externally imposed mean pressure gradient, i.e.

$$\left. \frac{\partial p}{\partial x} \right|_{mean} = 0. \quad (2.2f)$$

Mean flow rate $Q|_{mean}$ evaluated as

$$Q(t, X)|_{mean} = \left[\int_{Y_L(t, X)}^{Y_U(t, X)} u(t, X, Y) dY \right]_{mean} \quad (2.3)$$

provides a means for analysis of pumping effectiveness.

2.3 Determination of stresses and forces

Description of the flow mechanics requires knowledge of surface forces acting on the fluid at the walls. The description will start with the lower wall and specifically with the determination of the stress vector $\vec{\sigma}_L$,

$$\vec{\sigma}_L = [\sigma_{X,L} \quad \sigma_{Y,L}] = [n_{X,L} \quad n_{Y,L}] \begin{bmatrix} 2 \frac{\partial u}{\partial X} - p & \frac{\partial u}{\partial Y} + \frac{\partial v}{\partial X} \\ \frac{\partial u}{\partial Y} + \frac{\partial v}{\partial X} & 2 \frac{\partial v}{\partial Y} - p \end{bmatrix}_{Y=Y_L}, \quad (2.4)$$

where the normal unit vector \vec{n}_L pointing outwards is expressed as

$$\vec{n}_L = (n_{X,L}, n_{Y,L}) = N_L \left(\frac{dY_L}{dX}, -1 \right), \quad N_L = \left[1 + \left(\frac{dY_L}{dX} \right)^2 \right]^{-\frac{1}{2}} \quad (2.5)$$

The components of the stress vector can be written explicitly as follows:

$$\sigma_{X,L} = \sigma_{Xv,L} + \sigma_{Xp,L} = N_L \left[2 \frac{dY_L}{dX} \frac{\partial u}{\partial X} \Big|_{Y_L} - \left(\frac{\partial u}{\partial Y} + \frac{\partial v}{\partial X} \right) \Big|_{Y_L} \right] - N_L \frac{dY_L}{dX} p \Big|_{Y_L}, \quad (2.6a)$$

$$\sigma_{Y,L} = \sigma_{Yv,L} + \sigma_{Yp,L} = N_L \left[\frac{dY_L}{dX} \left(\frac{\partial u}{\partial Y} + \frac{\partial v}{\partial X} \right) \Big|_{Y_L} - 2 \frac{\partial v}{\partial Y} \Big|_{Y_L} \right] + N_L p \Big|_{Y_L}, \quad (2.6b)$$

where $(\sigma_{Xv,L}, \sigma_{Yv,L})$ and $(\sigma_{Xp,L}, \sigma_{Yp,L})$ denote the viscous and pressure contributions, respectively. Similarly, the normal $(\sigma_{n,L})$ and tangential $(\sigma_{t,L})$ components can be expressed as

$$\sigma_{n,L} = \sigma_{nv,L} + \sigma_{np,L} = 2N_L^2 \left[\left(\frac{dY_L}{dX} \right)^2 \frac{\partial u}{\partial X} \Big|_{Y_L} - \frac{dY_L}{dX} \left(\frac{\partial u}{\partial Y} + \frac{\partial v}{\partial X} \right) \Big|_{Y_L} + \frac{\partial v}{\partial Y} \Big|_{Y_L} \right] - p \Big|_{Y_L}, \quad (2.7a)$$

$$\sigma_{t,L} = N_L^2 \left\{ 2 \frac{dY_L}{dX} \left(\frac{\partial u}{\partial X} - \frac{\partial v}{\partial Y} \right) \Big|_{Y_L} - \left[1 - \left(\frac{dY_L}{dX} \right)^2 \right] \left(\frac{\partial u}{\partial Y} + \frac{\partial v}{\partial X} \right) \Big|_{Y_L} \right\}, \quad (2.7b)$$

where $\sigma_{nv,L}$ and $\sigma_{np,L}$ denote the viscous and pressure contributions, respectively. The X - and Y -components of the total force $(F_{X,L}, F_{Y,L})$ acting on the fluid at the lower wall per its unit length can be determined as

$$F_{X,L} = F_{Xv,L} + F_{Xp,L} = \lambda^{-1} \int_{X_0}^{X_0+\lambda} \left[2 \frac{dY_L}{dX} \frac{\partial u}{\partial X} \Big|_{Y_L} - \left(\frac{\partial u}{\partial Y} + \frac{\partial v}{\partial X} \right) \Big|_{Y_L} \right] dX - \lambda^{-1} \int_{X_0}^{X_0+\lambda} \frac{dY_L}{dX} p \Big|_{Y_L} dX, \quad (2.8a)$$

$$F_{Y,L} = F_{Yv,L} + F_{Yp,L} = \lambda^{-1} \int_{X_0}^{X_0+\lambda} \left[\frac{dY_L}{dX} \left(\frac{\partial u}{\partial Y} + \frac{\partial v}{\partial X} \right) \Big|_{Y_L} - 2 \frac{\partial v}{\partial Y} \Big|_{Y_L} \right] dX + \lambda^{-1} \int_{X_0}^{X_0+\lambda} p \Big|_{Y_L} dX, \quad (2.8b)$$

where X_0 is a convenient reference point and integration extends over one wavelength, $F_{Xp,L}$ and $F_{Yp,L}$ denote the pressure contributions while $F_{Xv,L}$ and $F_{Yv,L}$ stand for the viscous contributions.

The similar process applied to the upper wall leads to

$$\vec{\sigma}_U = [\sigma_{X,U} \quad \sigma_{Y,U}] = [n_{X,U} \quad n_{Y,U}] \begin{bmatrix} 2 \frac{\partial u}{\partial X} - p & \frac{\partial u}{\partial Y} + \frac{\partial v}{\partial X} \\ \frac{\partial u}{\partial Y} + \frac{\partial v}{\partial X} & 2 \frac{\partial v}{\partial Y} - p \end{bmatrix}_{Y=Y_U}, \quad (2.9)$$

where the normal unit vector \vec{n}_U pointing outwards is expressed as

$$\vec{n}_U = (n_{X,U}, n_{Y,U}) = N_U \left(-\frac{dY_U}{dX}, 1 \right), \quad N_U = \left[1 + \left(\frac{dY_U}{dX} \right)^2 \right]^{-\frac{1}{2}} \quad (2.10)$$

The components of the stress vector are expressed as

$$\sigma_{X,U} = \sigma_{Xv,U} + \sigma_{Xp,U} = N_U \left[-2 \frac{dY_U}{dX} \frac{\partial u}{\partial X} \Big|_{Y_U} + \left(\frac{\partial u}{\partial Y} + \frac{\partial v}{\partial X} \right) \Big|_{Y_U} \right] + N_U \frac{dY_U}{dX} p \Big|_{y_U}, \quad (2.11a)$$

$$\sigma_{Y,U} = \sigma_{Yv,U} + \sigma_{Yp,U} = N_U \left[-\frac{dY_U}{dX} \left(\frac{\partial u}{\partial Y} + \frac{\partial v}{\partial X} \right) \Big|_{Y_U} + 2 \frac{\partial v}{\partial Y} \Big|_{Y_U} \right] - N_U p \Big|_{y_U}, \quad (2.11b)$$

where $(\sigma_{Xv,U}, \sigma_{Yv,U})$ and $(\sigma_{Xp,U}, \sigma_{Yp,U})$ denote the viscous and pressure contributions, respectively. Similarly, the normal $(\sigma_{n,U})$ and tangential $(\sigma_{t,U})$ components can be expressed as

$$\sigma_{n,U} = \sigma_{nv,U} + \sigma_{np,U} = 2N_U^2 \left[\left(\frac{dY_U}{dX} \right)^2 \frac{\partial u}{\partial X} \Big|_{Y_U} - \frac{dY_U}{dX} \left(\frac{\partial u}{\partial Y} + \frac{\partial v}{\partial X} \right) \Big|_{Y_U} + \frac{\partial v}{\partial Y} \Big|_{Y_U} \right] - p \Big|_{y_U}, \quad (2.12a)$$

$$\sigma_{t,U} = N_U^2 \left\{ 2 \frac{dY_U}{dX} \left(\frac{\partial u}{\partial X} - \frac{\partial v}{\partial Y} \right) \Big|_{Y_U} - \left[1 - \left(\frac{dY_U}{dX} \right)^2 \right] \left(\frac{\partial u}{\partial Y} + \frac{\partial v}{\partial X} \right) \Big|_{Y_U} \right\}, \quad (2.12b)$$

where $\sigma_{nv,U}$ and $\sigma_{np,U}$ denote the viscous and pressure contributions, respectively. The X - and Y -components of the total force $(F_{X,U}, F_{Y,U})$ acting on the fluid at the upper wall per its unit length can be determined as

$$F_{X,U} = F_{Xv,U} + F_{Xp,U} = \lambda^{-1} \int_{X_0}^{X_0+\lambda} \left[-2 \frac{dY_U}{dX} \frac{\partial u}{\partial X} \Big|_{Y_U} + \left(\frac{\partial u}{\partial Y} + \frac{\partial v}{\partial X} \right) \Big|_{Y_U} \right] dX + \lambda^{-1} \int_{X_0}^{X_0+\lambda} \frac{dY_U}{dX} p \Big|_{Y_U} dX, \quad (2.13a)$$

$$F_{Y,U} = F_{Yv,U} + F_{Yp,U} = \lambda^{-1} \int_{X_0}^{X_0+\lambda} \left[-\frac{dY_U}{dX} \left(\frac{\partial u}{\partial Y} + \frac{\partial v}{\partial X} \right) \Big|_{Y_U} + 2 \frac{\partial v}{\partial Y} \Big|_{Y_U} \right] dX - \lambda^{-1} \int_{X_0}^{X_0+\lambda} p \Big|_{Y_U} dX, \quad (2.13b)$$

where $F_{Xp,U}$ and $F_{Yp,U}$ denote the pressure contributions while $F_{Xv,U}$ and $F_{Yv,U}$ stand for the viscous contributions.

The total force H_{tot} acting on the fluid at both walls per unit slot length must be zero and its evaluation according to the relation

$$H_{tot} = [H_{tot,X}, H_{tot,Y}] = [(F_{X,L} + F_{X,U}), (F_{Y,L} + F_{Y,U})] \quad (2.14)$$

serves as a useful check for the integrity of the numerical solution.

2.4 Introducing Galileo transformation

How the introduction of Galileo transformation simplifies the problem is described in this subsection. The form of the governing equations, boundary conditions, equation of flow

constraint, and location of boundaries after introducing Galileo transformation are also presented here. The analysis is simplified by introducing a frame of reference moving with wave phase speed. The relevant Galileo transformation has the form

$$y = Y, \quad x = X - ct. \quad (2.15)$$

Its use leads to a steady problem of the form

$$(u - c) \frac{\partial u}{\partial x} + v \frac{\partial u}{\partial y} = -\frac{\partial p}{\partial x} + \frac{\partial^2 u}{\partial x^2} + \frac{\partial^2 u}{\partial y^2}, \quad (2.16a)$$

$$(u - c) \frac{\partial v}{\partial x} + v \frac{\partial v}{\partial y} = -\frac{\partial p}{\partial y} + \frac{\partial^2 v}{\partial x^2} + \frac{\partial^2 v}{\partial y^2}, \quad (2.16b)$$

$$\frac{\partial u}{\partial x} + \frac{\partial v}{\partial y} = 0, \quad (2.16c)$$

$$y = y_U(x): \quad u = 0, \quad v = -c \frac{dy_U}{dx}, \quad (2.16d)$$

$$y = y_L(x): \quad u = 0, \quad v = -c \frac{dy_L}{dx}, \quad (2.16e)$$

$$\left. \frac{\partial p}{\partial x} \right|_{mean} = 0, \quad (2.16f)$$

where locations of the boundaries are given as

$$y_U(x) = 1 + B_U \sum_{n=-N_A}^{n=N_A} H_U^{(n)} e^{inax}, \quad y_L(x) = -1 + B_L \sum_{n=-N_A}^{n=N_A} H_L^{(n)} e^{inax} \quad (2.16g-h)$$

Chapter 3

3 Numerical Solution

This chapter introduces the procedure used in the numerical solution.

3.1 Introducing function ψ

Analysis of waves with arbitrary forms requires the use of numerical methods. As the first step, equations are re-arranged into a form suitable for numerical solution, i.e. function ψ is introduced which can be defined as

$$u = \frac{\partial \psi}{\partial y}, \quad v = -\frac{\partial \psi}{\partial x} \quad (3.1)$$

which eliminates the continuity equation.

3.1.1 Governing equation after introducing function ψ

Now, the pressure is eliminated by taking the derivative of (2.16a) with respect to y and the derivative of (2.16b) with respect to x and subtracting the resulting relations. The resulting flow problem has the form

$$\nabla^2(\nabla^2\psi) + c \frac{\partial}{\partial x} \nabla^2\psi = N_{uv} \quad \text{where} \quad N_{uv} = \frac{\partial}{\partial y} \left(\frac{\partial}{\partial x} \widehat{u}u + \frac{\partial}{\partial y} \widehat{u}v \right) - \frac{\partial}{\partial x} \left(\frac{\partial}{\partial x} \widehat{u}v + \frac{\partial}{\partial y} \widehat{v}v \right), \quad (3.2a)$$

In the above, hats denote products of quantities under the hat.

3.1.2 Boundary conditions after introducing function ψ and equation of constraint

The following form of boundary conditions are obtained after introducing function ψ

$$y = y_U(x): \quad \frac{\partial \psi}{\partial y} = 0, \quad \frac{\partial \psi}{\partial x} = c \frac{dy_U}{dx}, \quad (3.2b,c)$$

$$y = y_L(x): \quad \frac{\partial \psi}{\partial y} = 0, \quad \frac{\partial \psi}{\partial x} = c \frac{dy_L}{dx}, \quad (3.2d,e)$$

$$\left. \frac{\partial p}{\partial x} \right|_{mean} = 0. \quad (2.16f)$$

3.1.3 Function ψ along the boundaries

Condition (3.2e) can be written in a different form by noting that variations of ψ along the lower wall can be expressed as

$$d\psi_L = \left(\frac{\partial \psi}{\partial x} dx + \frac{\partial \psi}{\partial y} dy \right) \Big|_{y_L(x)} = c \frac{dy_L}{dx} dx. \quad (3.3)$$

Integration along the wall results in

$$\psi_L(x) = c[y_L(x) - y_L(x_0)] \quad (3.4)$$

where the constant of integration has been selected by assuming that $\psi_L(x_0) = 0$ with x_0 representing an arbitrary point on the lower wall. As ψ is defined with accuracy up to a constant (it is defined by velocity derivatives), this condition results in selecting this constant. A similar analysis carried out for the upper wall leads to expression of the form

$$\psi_U(x) = c[y_U(x) - y_U(x_0)] + const \quad (3.5)$$

where *const* needs to be determined from the pressure gradient constraint.

3.2 Discretization Method

The discretization procedure is described in this subsection.

The Chebyshev and Fourier expansions are used to provide a spectrally accurate discretization of the field equations (Canuto et al, 2006). Preference is given to use the standard definitions of Chebyshev polynomials involving domain $y \in (-1,1)$. Since the computational domain extends beyond these limits, transformation is introduced in the form

$$\hat{y} = 2 \left[\frac{y - (1 + y_t)}{y_t + y_b + 2} \right] + 1 \quad (3.6)$$

which maps the strip $y \in (-1 - y_b, 1 + y_t)$ in the y -direction into the strip $\hat{y} \in (-1,1)$ in the \hat{y} -direction. Here y_t and y_b denote locations of extremities of the upper and lower walls, respectively. As a result, the flow domain is completely immersed in the computational domain.

3.2.1 Discretization of governing equations

The field equations and boundary condition expressed using the \hat{y} - rather than the y -coordinate have the form

$$\begin{aligned} \Gamma^4 \frac{\partial^4 \psi}{\partial \hat{y}^4} + 2\Gamma^2 \frac{\partial^2}{\partial x^2} \left(\frac{\partial^2 \psi}{\partial \hat{y}^2} \right) + \frac{\partial^4 \psi}{\partial x^4} + c \frac{\partial}{\partial x} \left(\frac{\partial^2 \psi}{\partial x^2} + \Gamma^2 \frac{\partial^2 \psi}{\partial \hat{y}^2} \right) = \Gamma \frac{\partial}{\partial \hat{y}} \left(\frac{\partial}{\partial x} \widehat{u} \widehat{u} + \Gamma \frac{\partial}{\partial \hat{y}} \widehat{u} \widehat{v} \right) - \\ \frac{\partial}{\partial x} \left(\frac{\partial}{\partial x} \widehat{u} \widehat{v} + \Gamma \frac{\partial}{\partial \hat{y}} \widehat{v} \widehat{v} \right), \end{aligned} \quad (3.7a)$$

$$\hat{y} = \hat{y}_U(x): \quad \frac{\partial \psi}{\partial \hat{y}} = 0, \quad (3.7b)$$

$$\frac{\partial \psi}{\partial x} = c \frac{d\hat{y}_U}{dx} \text{ or } \psi(x) = c\Gamma^{-1}[\hat{y}_U(x) - \hat{y}_L(x_0)] - 2c, \quad (3.7c)$$

$$\hat{y} = \hat{y}_L(x): \quad \frac{\partial \psi}{\partial \hat{y}} = 0, \quad (3.7d)$$

$$\frac{\partial \psi}{\partial x} = c \frac{d\hat{y}_L}{dx} \text{ or } \psi(x) = c\Gamma^{-1}[\hat{y}_L(x) - \hat{y}_L(x_0)] \quad (3.7e)$$

where the locations of the boundaries are given as

$$\hat{y}_U = \sum_{n=-N_A}^{N_A} A_U^{(n)} e^{inax} \text{ with } A_U^{(0)} = 1 - \Gamma y_t + \Gamma B_U H_U^{(0)}, \quad A_U^{(n)} = \Gamma H_U^{(n)} \quad \text{for } n \neq 0, \quad (3.7f)$$

$$\hat{y}_L = \sum_{n=-N_A}^{N_A} A_L^{(n)} e^{inax} \text{ with } A_L^{(0)} = 1 + \Gamma(-2 - y_t) + \Gamma B_L H_L^{(0)}, \quad A_L^{(n)} = \Gamma H_L^{(n)} \quad \text{for } n \neq 0. \quad (3.7g)$$

In the above, $\Gamma = \frac{d\hat{y}}{dy} = \frac{2}{y_t + y_b + 2}$ and $A_U^{(n)} = A_U^{(-n)*}$ and $A_L^{(n)} = A_L^{(-n)*}$ represent the reality conditions. (3.8)

Since waves are periodic, all unknowns can be expressed as Fourier expansions of the form

$$q(x, \hat{y}) = \sum_{m=-N_M}^{m=+N_M} q^{(m)}(\hat{y}) e^{imax} \quad (3.9)$$

where q stands for any of the following quantities: $\psi, v, u, p, \widehat{v\bar{v}}, \widehat{u\bar{u}}, \widehat{u\bar{v}}$, the modal functions $q^{(m)}(\hat{y})$ satisfy the reality conditions, i.e. $q^{(m)}$ is the complex conjugate of $q^{(-m)}$, and $N_M > N_A$ with its acceptable value to be determined through numerical convergence studies. Substitution of (3.9) into (3.7a) and separation of Fourier components lead to the following equations for the modal functions $\psi^{(m)}$

$$[\Gamma^4 D^4 - 2m^2 \alpha^2 \Gamma^2 D^2 + m^4 \alpha^4] \psi^{(m)}(\hat{y}) + imac[\Gamma^2 D^2 - m^2 \alpha^2] \psi^{(m)}(\hat{y}) = im\alpha \Gamma D \widehat{u\bar{u}}^{(m)}(\hat{y}) + [\Gamma^2 D^2 + m^2 \alpha^2] \widehat{u\bar{v}}^{(m)}(\hat{y}) - im\alpha \Gamma D \widehat{v\bar{v}}^{(m)}(\hat{y}), \quad (3.10)$$

where $D = \frac{d}{d\hat{y}}$, $-N_M \leq m \leq N_M$ and terms on the right-hand side originate from the nonlinearities. To convert (3.10) into algebraic equations, the modal functions are represented as Chebyshev expansions of the form

$$\begin{aligned} & [\psi^{(m)}, \widehat{uu}^{(m)}, \widehat{uv}^{(m)}, \widehat{vv}^{(m)}, u^{(m)}, v^{(m)}, p^{(m)}](\hat{y}) \\ & \approx \sum_{k=0}^{N_T-1} \left[G\psi_k^{(m)}, G\widehat{uu}_k^{(m)}, G\widehat{uv}_k^{(m)}, G\widehat{vv}_k^{(m)}, Gu_k^{(m)}, Gv_k^{(m)}, GP_k^{(m)} \right] T_k(\hat{y}). \end{aligned} \quad (3.11)$$

(3.11) is substituted into (3.10) and the Galerkin projection method is used to construct the linear algebraic equations for the Chebyshev expansion coefficients. The algebraic equations have the following form

$$\begin{aligned} & \sum_{k=0}^{N_T-1} \{ (\Gamma^4 \langle T_j, D^4 T_k \rangle - 2m^2 \alpha^2 \Gamma^2 \langle T_j, D^2 T_k \rangle + m^4 \alpha^4 \langle T_j, T_k \rangle) + im\alpha c (\Gamma^2 \langle T_j, D^2 T_k \rangle - \\ & m^2 \alpha^2 \langle T_j, T_k \rangle) \} G\psi_k^{(m)} = \sum_{k=0}^{N_T-1} \left[im\alpha \Gamma \langle T_j, DT_k \rangle G\widehat{uu}_k^{(m)} + (\Gamma^2 \langle T_j, D^2 T_k \rangle + \right. \\ & \left. m\alpha^2 \langle T_j, T_k \rangle) G\widehat{uv}_k^{(m)} - im\alpha \Gamma \langle T_j, DT_k \rangle G\widehat{vv}_k^{(m)} \right] \end{aligned} \quad (3.12)$$

where $0 \leq k, j \leq N_T - 1$, $-N_M \leq m \leq N_M$ and the inner products are defined as $\langle f(\hat{y}), g(\hat{y}) \rangle = \int_{-1}^1 f(\hat{y}) g(\hat{y}) \omega(\hat{y}) d\hat{y}$ where $\omega(\hat{y}) = \frac{1}{\sqrt{1-\hat{y}^2}}$ is the weight function.

3.2.2 Discretization of boundary conditions and pressure gradient constraint

Spectral methods are not suitable for handling of irregular geometries. This difficulty can be overcome by implementing the immersed boundaries (IBC) concept. The method that

is followed here is described by Husain and Floryan (2008, 2010), Husain et al (2009), Zandi et al (2015), and Moradi et al (2017).

The boundary conditions are imposed using the tau concept (Canuto et al, 2006). Four equations resulting from the discretization of each modal equation (3.12) corresponding to the highest Chebyshev polynomials are eliminated to provide space for the inclusion of the boundary conditions.

Discretization of boundary conditions at the upper wall starts with substituting (3.9) and (3.11) into (3.2b, c) resulting in

$$\left. \frac{\partial \psi}{\partial \hat{y}} \right|_{\hat{y}_U} = \sum_{n=-N_M}^{N_M} D\psi^{(n)}(\hat{y}_U(x))e^{in\alpha x} = \sum_{n=-N_M}^{N_M} \sum_{k=0}^{N_T-1} G\psi_k^{(n)} DT_k(\hat{y}_U(x))e^{in\alpha x}, \quad (3.13a)$$

$$\left. \frac{\partial \psi}{\partial x} \right|_{\hat{y}_U} = \sum_{n=-N_M}^{N_M} in\alpha \psi^{(n)}(\hat{y}_U(x))e^{in\alpha x} = \sum_{n=-N_M}^{N_M} \sum_{k=0}^{N_T-1} in\alpha G\psi_k^{(n)} T_k(\hat{y}_U(x))e^{in\alpha x}. \quad (3.13b)$$

Taking the Fourier expansion of Chebyshev polynomials and their derivatives from (3.13) the following are obtained:

[detail derivation of these relations is given in Appendix A]

$$\begin{aligned} \frac{\partial \psi}{\partial \hat{y}} &= \sum_{n=-N_M}^{N_M} \sum_{k=0}^{N_T-1} \sum_{m=-N_S}^{N_S} G\psi_k^{(n)} (d_U)_k^{(m)} e^{i(n+m)\alpha x} = \\ &\sum_{h=-N_S-N_M}^{N_S+N_M} \sum_{n=-N_M}^{N_M} \sum_{k=0}^{N_T-1} G\psi_k^{(n)} (d_U)_k^{(h-n)} e^{ih\alpha x}, \end{aligned} \quad (3.14a)$$

$$\begin{aligned} \frac{\partial \psi}{\partial x} &= i\alpha \sum_{n=-N_M}^{N_M} \sum_{k=0}^{N_T-1} \sum_{m=-N_S}^{N_S} nG\psi_k^{(n)} (w_U)_k^{(m)} e^{i(n+m)\alpha x} \\ &= i\alpha \sum_{h=-N_S-N_M}^{N_S+N_M} \sum_{n=-N_M}^{N_M} \sum_{k=0}^{N_T-1} nG\psi_k^{(n)} (w_U)_k^{(h-n)} e^{ih\alpha x} \end{aligned} \quad (3.14b)$$

where $h = n + m$. It can be deduced that $(w_U)_k^{(h-n)}$ and $(d_U)_k^{(h-n)}$ take the non-zero values only for $|h - n| \leq N_s$. Redefining the indices $n \rightarrow m$ and $h \rightarrow n$ in (3.14) and substituting them into (3.7b, c) and use of (3.7f), lead to boundary relations of the form

$$\sum_{m=-N_M}^{N_M} \sum_{k=0}^{N_T-1} G\psi_k^{(m)}(d_U)_k^{(n-m)} = 0 \quad \text{for } 0 \leq |n| \leq N_f, \quad (3.15a)$$

$$\sum_{m=-N_M}^{N_M} \sum_{k=0}^{N_T-1} im\alpha G\psi_k^{(m)}(w_U)_k^{(n-m)} = in\alpha c\Gamma^{-1}A_U^{(n)} \quad \text{for } 1 \leq |n| \leq N_f, \quad (3.15b)$$

where $N_f = (N_T - 1)N_A + N_M$.

A similar process applied at the lower wall leads to the following relations

$$\sum_{m=-N_M}^{N_M} \sum_{k=0}^{N_T-1} G\psi_k^{(m)}(d_L)_k^{(n-m)} = 0 \quad \text{for } 0 \leq |n| \leq N_f, \quad (3.16a)$$

$$\sum_{m=-N_M}^{N_M} \sum_{k=0}^{N_T-1} im\alpha G\psi_k^{(m)}(w_L)_k^{(n-m)} = in\alpha c\Gamma^{-1}A_L^{(n)} \quad \text{for } 1 \leq |n| \leq N_f. \quad (3.16b)$$

Relations (3.15b) and (3.16b) do not provide conditions for $n = 0$ which is due to the character of the boundary conditions for v . The first missing condition can be constructed by substituting (3.7g) into (3.7e) and taking $x_0 = 0$ leading to

$$\psi_L = c\Gamma^{-1} \sum_{n=-N_M}^{n=N_M} A_L^{(n)} e^{inax} - c\Gamma^{-1} \sum_{n=-N_M}^{n=N_M} A_L^{(n)} \quad (3.17)$$

where ψ_L denotes the value of ψ at the lower wall. ψ can also be expressed at this wall using (3.9), (3.11), i.e.

$$\psi_L = \sum_{n=-N_f}^{N_f} \sum_{m=-N_M}^{N_M} \sum_{k=0}^{N_T-1} G\psi_k^{(m)}(w_L)_k^{(n-m)} e^{inax}. \quad (3.18)$$

Equating (3.17) with (3.18) and extracting mode zero leads to the final form of this condition

$$\sum_{m=-N_M}^{N_M} \sum_{k=0}^{N_T-1} G \psi_k^{(m)} (w_L)_k^{(m)*} = c \Gamma^{-1} \left(A_L^{(0)} - \sum_{n=-N_M}^{N_M} A_L^{(n)} \right). \quad (3.19)$$

The fixed pressure gradient constraint (2.16f) is used to construct the second missing condition. It is going to be started with the determination of the pressure field assuming that the velocity field is known. Use of the x -momentum equation (2.16a) written in the (x, \hat{y}) -coordinates lead to

$$\frac{\partial p}{\partial x} = -\frac{\partial \langle uu \rangle}{\partial x} - \Gamma \frac{\partial \langle uv \rangle}{\partial \hat{y}} + \frac{\partial^2 u}{\partial x^2} + \Gamma^2 \frac{\partial^2 u}{\partial \hat{y}^2} + c \frac{\partial u}{\partial x}. \quad (3.20)$$

Substitution of (3.9) into (3.20) and separation of Fourier modes results in

$$\begin{aligned} im\alpha p^{(m)}(\hat{y}) = & -im\alpha \langle uu \rangle^{(m)}(\hat{y}) - \Gamma D \langle uv \rangle^{(m)}(\hat{y}) - m^2 \alpha^2 \Gamma D \psi^{(m)}(\hat{y}) + \\ & \Gamma^3 D^3 \psi^{(m)}(\hat{y}) + c im\alpha \Gamma D \psi^{(m)}(\hat{y}) \end{aligned} \quad (3.21)$$

which can be used to determine pressure modal functions $p^{(m)}(\hat{y})$ for any m , except $m = 0$. The actual computations involve the substitution of Chebyshev expansions for all terms, taking the inner products with $T_j(\hat{y})$ and using orthogonality properties to arrive at

$$\begin{aligned} GP_k^{(m)} = & 2(im\alpha\pi C_j)^{-1} \sum_{k=0}^{N_T-1} \left\{ -im\alpha G \widehat{uu}_k^{(m)} \langle T_j, T_k \rangle - \Gamma G \widehat{uv}_k^{(m)} \langle T_j, DT_k \rangle + \right. \\ & \left. c im\alpha \Gamma G \psi_k^{(m)} \langle T_j, DT_k \rangle + \Gamma G \psi_k^{(m)} [-m^2 \alpha^2 \langle T_j, DT_k \rangle + \Gamma^2 \langle T_j, D^3 T_k \rangle] \right\} \end{aligned} \quad (3.22)$$

$$\text{where } C_j = \begin{cases} 2 & \text{for } j = 0, \\ 1 & \text{for } j \neq 0, \end{cases} \quad \text{for } \begin{cases} m \neq 0, \\ 0 \leq j \leq N_T - 1. \end{cases}$$

Determination of mode zero requires the use of the y -momentum equation (2.16b) written in the (x, \hat{y}) -coordinates which have the following form

$$\Gamma \frac{\partial P}{\partial \hat{y}} = -\frac{\partial \langle uv \rangle}{\partial x} - \Gamma \frac{\partial \langle vv \rangle}{\partial \hat{y}} + \frac{\partial^2 v}{\partial x^2} + \Gamma^2 \frac{\partial^2 v}{\partial \hat{y}^2} + c \frac{\partial v}{\partial x}. \quad (3.23)$$

Substitution of (3.9) into (3.23) and separation of Fourier modes result in

$$\begin{aligned} \Gamma DP^{(m)}(\hat{y}) &= -im\alpha \langle uv \rangle^{(m)}(\hat{y}) - \Gamma D \langle vv \rangle^{(m)}(\hat{y}) + im^3 \alpha^3 \psi^{(m)}(\hat{y}) - \\ &im\alpha \Gamma^2 D^2 \psi^{(m)}(\hat{y}) + c m^2 \alpha^2 \psi^{(m)}(\hat{y}) \end{aligned} \quad (3.24)$$

which reduces for mode zero to

$$DP^{(0)}(\hat{y}) = -D \langle vv \rangle^{(0)}(\hat{y}) \quad (3.25)$$

which, after integration, becomes

$$P^{(0)}(\hat{y}) = -\langle vv \rangle^{(0)}(\hat{y}) - C_1 \quad (3.26)$$

where C_1 stands for an arbitrary constant. Substitution of Chebyshev expansions into (3.26), taking inner products with $T_j(\hat{y})$ and use of orthogonality properties results in

$$GP_k^{(0)} = -2 (C_j \pi)^{-1} \sum_{k=0}^{N_T-1} G \widehat{vv}_k^{(0)} \langle T_j, T_k \rangle - 2 C_1 (C_j \pi)^{-1} \langle T_j, T_0 \rangle$$

$$\text{for } 0 \leq j \leq N_T - 1. \quad (3.27)$$

The complete pressure field for peristaltic pumping is given by

$$P(x, \hat{y}) = \sum_{m=-N_M}^{N_M} \sum_{k=0}^{N_T-1} GP_k^{(m)} T_k(\hat{y}) e^{imax}. \quad (3.28)$$

Extraction of mode zero from (3.21) provides the condition leading to the imposition of the zero mean pressure gradient constraint, i.e.

$$D^3\psi^{(0)} = \Gamma^{-2}D\widehat{uv}^{(0)}. \quad (3.29)$$

One integration gives the form of this constraint suitable for numerical implementation, i.e.

$$D^2\psi^{(0)}(1) - D^2\psi^{(0)}(-1) = \Gamma^{-2}[\widehat{uv}^{(0)}(1) - \widehat{uv}^{(0)}(-1)]. \quad (3.30)$$

This constraint involves both ends of the solution domain.

3.3 Solution Process

The solution procedure is described in this subsection in two parts i.e., iterative solution process and method of updating nonlinear terms.

3.3.1 Iterative solution process

The system (3.12) supplemented with boundary relations (3.15), (3.16), (3.19), and (3.30) is solved assuming that the right-hand side is known which makes this system linear. A very efficient algorithm that takes advantage of the structure of the coefficient matrix is described by Husain and Floryan (2013). Since the right-hand side of (3.12) is not known, the overall solution process relies on iterations and yields new approximations of $\psi^{(n)}(\hat{y})$, denoted as $[\psi^{(n)}(\hat{y})]^{(k)}$, at each iteration where the superscript k denotes the iteration number. The nonlinear terms on the right-hand side of (3.12) are taken from the previous iteration (these terms are ignored during the first iteration) resulting in the first-order fixed point method. The iteration process can be summarized as

$$[\psi^{(n)}]^{(k+1)} = [\psi^{(n)}]^{(k)} + RF \{ [\psi^{(n)}]^{(comp)} - [\psi^{(n)}]^{(k)} \} \quad (3.31)$$

where the superscript *comp* identifies the solution computed at the new iteration, and the process is controlled using the under-relaxation parameter *RF*. Typically, $RF < 0.1$ is used with its value decreasing with an increase of the wave amplitude and the phase speed. Iterations are stopped when the convergence criterion of the form

$$\left| [\psi^{(n)}]^{(k+1)} - [\psi^{(n)}]^{(k)} \right| / \left| [\psi^{(n)}]^{(k+1)} \right| < CONV \quad (3.32)$$

is satisfied, where $\left| [\psi^{(n)}]^{(k+1)} - [\psi^{(n)}]^{(k)} \right|$ is the L^2 norm of the difference between the solution vectors computed at two consecutive iterations and $\left| [\psi^{(n)}]^{(k+1)} \right|$ is the L^2 norm of the current solution vector. $CONV = 10^{-14}$ was used in all tests of the algorithm while $CONV = 10^{-10}$ is sufficient for physical studies.

3.3.2 Method of updating nonlinear terms

The nonlinear terms on the right-hand side of (3.12) need to be updated at the end of each iteration step. It is more efficient to evaluate the required products by transferring data to the physical space, carrying out the multiplications there, and transferring the results back into the Fourier space (Canuto et al, 2006). The new values of the velocity components of the form

$$u(x, \hat{y}) = \Gamma \sum_{n=-N_M}^{N_M} D\psi^{(n)}(\hat{y})e^{inax}, \quad v(x, \hat{y}) = -i\alpha \sum_{n=-N_M}^{N_M} n\psi^{(n)}(\hat{y})e^{inax} \quad (3.33)$$

are computed on a suitable grid in the (x, \hat{y}) plane. $2N_x + 2$ equidistant points, where $N_x = \frac{3}{2}N_M$, are used along the x -direction to remove the aliasing error with the last point removed due to periodicity, and N_T points are used in the \hat{y} -direction with the first and last points overlapping with the borders of the computational domain. Chebyshev points defined as $\hat{y}_j = \cos\left(\frac{j\pi}{N_T-1}\right)$, where $j = 1, 2, \dots, N_T - 2$, are used in the interior of the domain. This process results in the formation of two matrices containing values of u and v and their multiplication yields the desired products, i.e. $\widehat{uu}, \widehat{uv}, \widehat{vv}$. These products need to be expressed using Fourier expansions (3.9) which necessitates the determination of the modal functions $\widehat{uu}^{(n)}, \widehat{uv}^{(n)}, \widehat{vv}^{(n)}$. This is accomplished using the Fast Fourier Transform (*FFT*) at each \hat{y} -location; $2N_x + 1$ data points are used in the x -direction resulting in values of $2N_x + 1$ modal functions. Modal functions with indices in the range $[-N_M, N_M]$ are retained and the remaining ones are discarded as-part of the aliasing error control process (Canuto et al, 2006). The last step involves expressing each modal function in terms of a Chebyshev expansion, i.e. the evaluation of coefficients $G\widehat{uu}_k^{(n)}, G\widehat{uv}_k^{(n)}, G\widehat{vv}_k^{(n)}$. Since values of these functions are available at the \hat{y} -grid points, one can write the equation of type (3.11) for each point resulting in a system of the linear equation whose numerical solution determines the unknown expansion coefficients. The number of grid points determines the maximum length of the Chebyshev expansion. No de-aliasing is required in the Chebyshev direction if a sufficient number of polynomials are used.

3.4 Post-Processing

Evaluation of stresses and forces along the boundaries

The evaluation of various surface forces along the boundaries as described in this section.

The discussion begins with the lower wall, specifically with the unit normal vector along the lower wall. Normal unit vectors can be expressed as

$$\vec{n}_L = (n_{x,L}, n_{y,L}) = N_L \left(\frac{dy_L}{dx}, -1 \right) = \left[B_L \sum_{n=-N_A}^{n=N_A} H_L^{(n)} in \alpha e^{inax}, -1 \right] N_L \quad (3.34)$$

where

$$N_L = \left[1 + \left(\frac{dy_L}{dx} \right)^2 \right]^{-\frac{1}{2}} = \left[1 - (B_L \alpha)^2 \left\{ \sum_{n=-N_A}^{n=N_A} H_L^{(n)} n e^{inax} \right\}^2 \right]^{-\frac{1}{2}}.$$

Component of shear stress vector along the lower boundary given by the following equation:

$$\sigma_{Xv,L} = N_L \left[2 \frac{dy_L}{dx} \frac{\partial u}{\partial x} \Big|_{y_L} - \left(\frac{\partial u}{\partial y} + \frac{\partial v}{\partial x} \right) \Big|_{y_L} \right].$$

Substitution of u and v using (3.1) and making use of (3.9) and (3.11) gives

$$\begin{aligned} \sigma_{Xv,L} = & \left[1 - (B_L \alpha)^2 \left\{ \sum_{n=-N_A}^{n=N_A} H_L^{(n)} n e^{inax} \right\}^2 \right]^{-\frac{1}{2}} \\ & \left[2 \left\{ \alpha B_L \sum_{n=-N_A}^{n=N_A} H_L^{(n)} in e^{inax} \right\} \left\{ \Gamma \alpha \sum_{m=-NM}^{NM} \sum_{k=0}^{NT-1} (im) G \psi_k^{(m)} D T_K(\hat{y}) e^{imax} \right\} \Big|_{y_L} - \right. \\ & \left. \left[\sum_{m=-NM}^{NM} \left\{ \sum_{k=0}^{NT-1} \left(\Gamma^2 G \psi_k^{(m)} D^2 T_K(\hat{y}) - (im\alpha)^2 G \psi_k^{(m)} T_K(\hat{y}) \right) \right\} e^{imax} \right] \Big|_{y_L} \right]. \quad (3.35) \end{aligned}$$

The x -component of viscous force along the lower wall is given by:

$$F_{Xv,L} = \lambda^{-1} \int_{x_0}^{x_0+\lambda} \sigma_{Xv,L} dx \quad (3.36)$$

where $\sigma_{Xv,L}$ can be obtained from (3.35).

the x -component of normal stress generated due to pressure along the lower boundary is given by:

$$\begin{aligned} \sigma_{Xp,L} &= -N_L \frac{dy_L}{dx} p \Big|_{y_L} = -p|_{y_L} n_{x,L} \\ &= - \left[1 - (B_L \alpha)^2 \left\{ \sum_{n=-N_A}^{n=N_A} H_L^{(n)} n e^{in\alpha x} \right\}^2 \right]^{-\frac{1}{2}} \\ &B_L \sum_{n=-N_A}^{n=N_A} H_L^{(n)} in\alpha e^{in\alpha x} \left(\sum_{m=-N_M}^{N_M} \sum_{k=0}^{N_T-1} GP_k^{(m)} T_k(\hat{y}) e^{im\alpha x} \right) \Big|_{y_L}. \end{aligned} \quad (3.37)$$

Inserting (3.37) into (2.8a), the expression for evaluating x -component of pressure force acting along the lower boundary can be obtained as follows:

$$F_{Xp,L} = \lambda^{-1} \int_{x_0}^{x_0+\lambda} \sigma_{Xp,L} dx \quad (3.38)$$

where $\sigma_{Xp,L}$ can be obtained from (3.37).

Similarly, the expression for evaluating the y -component of viscous stress along the lower boundary is as follows:

$$\sigma_{Yv,L} = N_L \left[\frac{dy_L}{dx} \left(\frac{\partial u}{\partial y} + \frac{\partial v}{\partial x} \right) \Big|_{y_L} - 2 \frac{\partial v}{\partial y} \Big|_{y_L} \right]$$

$$\begin{aligned}
&= \left[1 - (B_L \alpha)^2 \left\{ \sum_{n=-N_A}^{n=N_A} H_L^{(n)} n e^{in\alpha x} \right\}^2 \right]^{-\frac{1}{2}} \\
&\left[B_L \sum_{n=-N_A}^{n=N_A} H_L^{(n)} in\alpha e^{in\alpha x} \left[\sum_{m=-N_M}^{N_M} \left\{ \sum_{k=0}^{N_T-1} \left(\Gamma^2 G \psi_k^{(m)} D^2 T_k(\hat{y}) - \right. \right. \right. \right. \\
&\left. \left. \left. (im\alpha)^2 G \psi_k^{(m)} T_k(\hat{y}) \right) \right\} e^{im\alpha x} \right] \Big|_{y_L} - 2\Gamma \sum_{m=-N_M}^{N_M} \sum_{k=0}^{N_T-1} (im\alpha) G \psi_k^{(m)} D T_k(\hat{y}) e^{im\alpha x} \Big|_{y_L} \right]. \quad (3.39)
\end{aligned}$$

The y -component of the viscous force acting along the lower boundary is determined as follows:

$$F_{Yv,L} = \lambda^{-1} \int_{x_0}^{x_0+\lambda} \sigma_{Yv,L} dx \quad (3.40)$$

where $\sigma_{Yv,L}$ can be obtained from (3.39).

Evaluation of the y -component of normal stress generated due to pressure at the lower boundary is obtained as follows

$$\begin{aligned}
\sigma_{Yp,L} &= N_L p|_{y_L} \\
&= \left[1 - (B_L \alpha)^2 \left\{ \sum_{n=-N_A}^{n=N_A} H_L^{(n)} n e^{in\alpha x} \right\}^2 \right]^{-\frac{1}{2}} \left(\sum_{m=-N_M}^{N_M} \sum_{k=0}^{N_T-1} G P_k^{(m)} T_k(\hat{y}) e^{im\alpha x} \right) \Big|_{y_L}. \quad (3.41)
\end{aligned}$$

The y -component of pressure force acting along the lower boundary is given by

$$F_{Yp,L} = \lambda^{-1} \int_{x_0}^{x_0+\lambda} \sigma_{Yp,L} dx \quad (3.42)$$

where $\sigma_{Yp,L}$ can be obtained from (3.41).

This is how the stress vectors and forces acting on fluid along the lower boundary can be determined. Following a similar procedure, these quantities can be determined for the upper boundary as well.

Evaluation of various surface forces along the upper wall:

Unit vectors along the upper wall:

The unit normal vector pointing outwards has the form

$$\vec{n}_U = (n_{x,U}, n_{y,U}) = N_U \left(-\frac{dy_U}{dx}, 1 \right) =$$

$$\left[\frac{-B_U \sum_{n=-N_A}^{n=N_A} H_U^{(n)} i n \alpha e^{i n \alpha x}}{\sqrt{1 + \left\{ B_U \sum_{n=-N_A}^{n=N_A} H_U^{(n)} i n \alpha e^{i n \alpha x} \right\}^2}}, \frac{1}{\sqrt{1 + \left\{ B_U \sum_{n=-N_A}^{n=N_A} H_U^{(n)} i n \alpha e^{i n \alpha x} \right\}^2}} \right]$$
(3.43)

$$\text{here, } N_U = \left[1 + \left(\frac{dy_U}{dx} \right)^2 \right]^{-\frac{1}{2}} = \left[1 - (B_U \alpha)^2 \left\{ \sum_{n=-N_A}^{n=N_A} H_U^{(n)} n e^{i n \alpha x} \right\}^2 \right]^{-\frac{1}{2}}.$$

Component of shear stress vector along the upper boundary given by the following equation:

$$\sigma_{Xv,U} = N_U \left[2 \frac{dy_U}{dx} \frac{\partial u}{\partial x} \Big|_{y_U} - \left(\frac{\partial u}{\partial y} + \frac{\partial v}{\partial x} \right) \Big|_{y_U} \right].$$

Substitution of u and v using (3.1) and making use of (3.9) and (3.11) gives

$$\sigma_{Xv,U} = \left[1 - (B_U \alpha)^2 \left\{ \sum_{n=-N_A}^{n=N_A} H_U^{(n)} n e^{i n \alpha x} \right\}^2 \right]^{-\frac{1}{2}}$$

$$\left[2 \left\{ \alpha B_U \sum_{n=-N_A}^{n=N_A} H_U^{(n)} n e^{i n \alpha x} \right\} \left\{ \Gamma \alpha \sum_{m=-N_M}^{N_M} \sum_{k=0}^{N_T-1} (i m) G \psi_k^{(m)} D T_k(\hat{y}) e^{i m \alpha x} \right\} \right]_{y_U} - \left[\sum_{m=-N_M}^{N_M} \left\{ \sum_{k=0}^{N_T-1} \left(\Gamma^2 G \psi_k^{(m)} D^2 T_k(\hat{y}) - (i m \alpha)^2 G \psi_k^{(m)} T_k(\hat{y}) \right) \right\} e^{i m \alpha x} \right]_{y_U}. \quad (3.44)$$

By integrating the stress over one wavelength, the x -component of the viscous force along the upper boundary can be determined as follows:

$$F_{Xv,U} = \lambda^{-1} \int_{x_0}^{x_0+\lambda} \sigma_{Xv,U} dx \quad (3.45)$$

where $\sigma_{Xv,U}$ can be obtained from (3.44).

Following a similar procedure of the lower wall, the equation for evaluating the x -component of normal stress generated due to pressure at the upper boundary can be obtained as follows:

$$\begin{aligned} \sigma_{Xp,U} &= -N_U \frac{dy_U}{dx} p \Big|_{y_U} = -p|_{y_U} n_{x,U} \\ &= - \left[1 - (B_U \alpha)^2 \left\{ \sum_{n=-N_A}^{n=N_A} H_U^{(n)} n e^{i n \alpha x} \right\}^2 \right]^{-\frac{1}{2}} \\ & B_U \sum_{n=-N_A}^{n=N_A} H_U^{(n)} i n \alpha e^{i n \alpha x} \left(\sum_{m=-N_M}^{N_M} \sum_{k=0}^{N_T-1} G P_k^{(m)} T_k(\hat{y}) e^{i m \alpha x} \right) \Big|_{y_U}. \end{aligned} \quad (3.46)$$

The x -component of pressure force acting along the upper wall is given by:

$$F_{Xp,U} = \lambda^{-1} \int_{x_0}^{x_0+\lambda} \sigma_{Xp,U} dx \quad (3.47)$$

where $\sigma_{Xp,U}$ can be obtained from (3.46).

Similarly, the equation for determining the y -component of viscous stress along the upper boundary can be obtained as follows:

$$\begin{aligned}
\sigma_{Yv,U} &= N_U \left[\frac{dy_U}{dx} \left(\frac{\partial u}{\partial y} + \frac{\partial v}{\partial x} \right) \Big|_{y_U} - 2 \frac{\partial v}{\partial y} \Big|_{y_U} \right] \\
&= \left[1 - (B_U \alpha)^2 \left\{ \sum_{n=-N_A}^{n=N_A} H_U^{(n)} n e^{inax} \right\}^2 \right]^{-\frac{1}{2}} \\
&\quad \left[B_U \sum_{n=-N_A}^{n=N_A} H_U^{(n)} in\alpha e^{inax} \left[\sum_{m=-N_M}^{N_M} \left\{ \sum_{k=0}^{N_T-1} \left(\Gamma^2 G \psi_k^{(m)} D^2 T_k(\hat{y}) - \right. \right. \right. \right. \\
&\quad \left. \left. \left. (im\alpha)^2 G \psi_k^{(m)} T_k(\hat{y}) \right) \right\} e^{im\alpha x} \right] \Big|_{y_U} - 2\Gamma \sum_{m=-N_M}^{N_M} \sum_{k=0}^{N_T-1} (im\alpha) G \psi_k^{(m)} D T_k(\hat{y}) e^{im\alpha x} \Big|_{y_U} \right].
\end{aligned} \tag{3.48}$$

The y -component of the viscous force along the upper boundary is as follows:

$$F_{Yv,U} = \lambda^{-1} \int_{x_0}^{x_0+\lambda} \sigma_{Yv,U} dx \tag{3.49}$$

where $\sigma_{Yv,U}$ can be obtained from (3.48).

Following the similar procedure of the lower wall, the expression for evaluation of the y -component of normal stress generated due to pressure at the upper boundary can be obtained as follows

$$\begin{aligned}
\sigma_{Yp,U} &= N_U p|_{y_U} = \left[1 - (B_U \alpha)^2 \left\{ \sum_{n=-N_A}^{n=N_A} H_U^{(n)} n e^{inax} \right\}^2 \right]^{-\frac{1}{2}} \\
&\quad \left(\sum_{m=-N_M}^{N_M} \sum_{k=0}^{N_T-1} G P_k^{(m)} T_k(\hat{y}) e^{im\alpha x} \right) \Big|_{y_U}.
\end{aligned} \tag{3.50}$$

Integration of stress over one wavelength gives the equation for the y-component of pressure force acting along the upper boundary:

$$F_{yp,U} = \lambda^{-1} \int_{x_0}^{x_0+\lambda} \sigma_{Yp,U} dx \quad (3.51)$$

where $\sigma_{Yp,U}$ can be obtained from (3.50).

Chapter 4

4 Results and Discussion

The results of various investigations carried out as a part of this thesis will be discussed in this chapter. It will start with the wave placed at one of the walls and symbol A is used for its amplitude.

4.1 Effect of the wave wavenumber

Change of the wave wavenumber is expected to affect the system performance as quantified by the flow rate. Figure 4a illustrates variations of the flow rate Q as a function of the wavenumber α . The flow rate is nearly constant for sufficiently small wavenumbers but starts increasing when the wavenumber increases beyond $\alpha \approx 1$. This increase is proportional to α^2 . Some form of saturation is expected in the limit of $\alpha \rightarrow \infty$ but this limit was not investigated due to limitations of the computational method used in the analysis. Figure 4b illustrates variations of various forces generated at the walls, i.e. the x -component of the pressure force $F_{Xp,L}$ acting on the fluid at the lower wall, and the x -components of the viscous forces acting on the fluid at the lower ($F_{Xv,L}$) and upper ($F_{Xv,U}$) walls. The pressure force is responsible for driving the fluid movement while the viscous forces resist this movement. These forces are in balance as verified by evaluation of all forces acting on a control volume extending over one wavelength in the streamwise direction. All forces reach constant limits for $\alpha \rightarrow 0$ but their magnitudes begin to increase rapidly when the wavenumber increases beyond $\alpha \approx 1$. Viscous forces are negative in this figure demonstrating that they oppose the fluid movement while pressure forces are positive demonstrating that they propel the fluid.

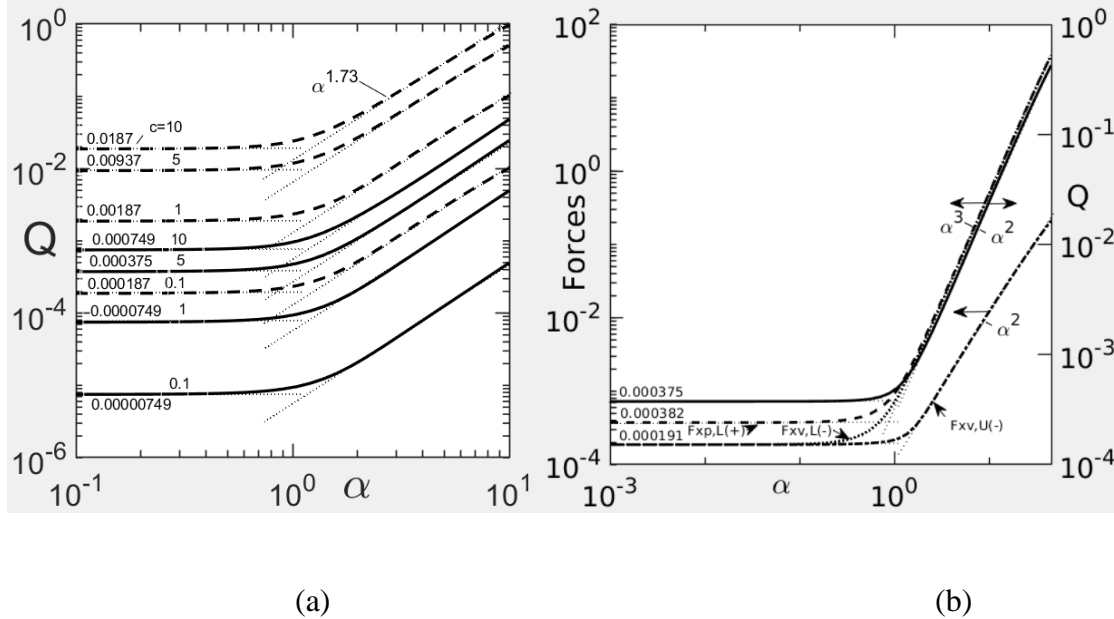


Figure 4.1 (a) Variation of the flow rate Q as a function of the wavenumber for different wave phase speeds c . Dashed and solid lines correspond to the wave amplitudes $A=0.05$ and 0.01 respectively. Dotted lines represent asymptotes. (b) Variations of the force components (the x -component of the shear force $F_{Xv,L}$ (dotted line), the x -component of the pressure force $F_{Xp,L}$ (dashed line) acting on the fluid at the lower wall and the x -component of the shear force $F_{Xv,U}$ (dash-dotted line) acting on the fluid at the upper wall) as functions of the wavenumber α . The variations of the flow rate Q are represented by solid lines. These computations are done for the amplitude $A = 0.01$ and the wave phase speed $c = 5$.

Variation of the flow rate can be divided into three regions, namely: small alpha region, big alpha region, and the region in between the two. In the small alpha region, variations of Q follow a certain asymptote and in the big alpha region, these variations follow another asymptote.

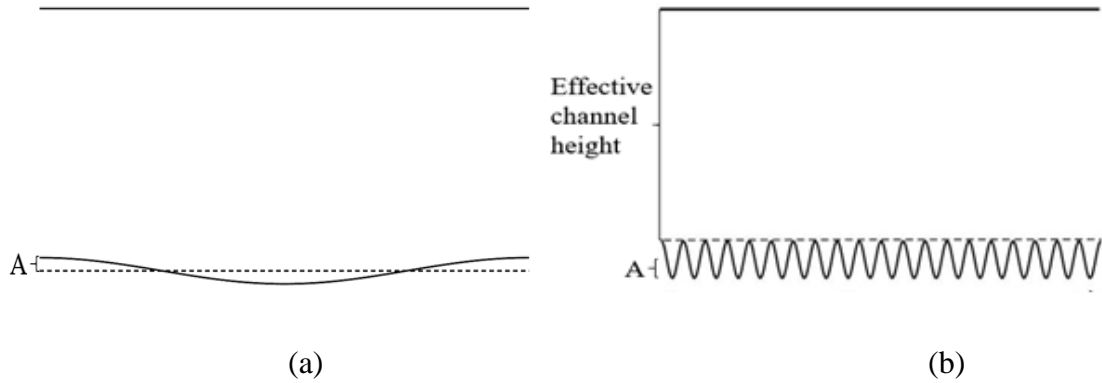


Figure 4.2 (a) Sketch of the lower wall with the small wavenumber waves; (b) Sketch of the lower wall with the large wavenumber waves.

From Fig 4.2(a), it can be deduced that at small wavenumbers the channel height changes very slowly and as a result, the flow rate remains almost constant. That is why in the region of small wavenumbers variations of the flow rate follow a “small alpha asymptote”.

Similarly, from Fig 4.2(b), it is noticed that when the wavenumber is large, then the effective channel height decreases while the wall appears to the fluid as a wall moving to the right resulting in the flow rate following a “big alpha asymptote”.

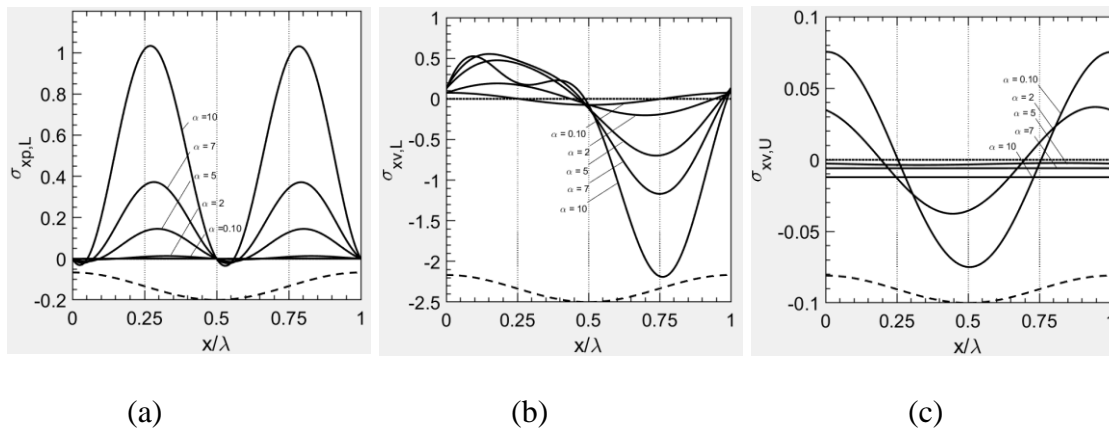


Figure 4.3 (a) Distribution of the x-component of the pressure force acting on the fluid at the lower wall over one wavelength, (b) Distribution of the x-component of the shear force acting on the fluid at the lower wall over one wavelength, (c) Distribution of the x-

component of the shear force acting on the fluid at the upper wall over one wavelength. In all plots, solid lines represent forces and the dashed lines represent wave shape. All these plots correspond to the wave amplitude $A = 0.01$ and the wave phase speed $c = 5$.

Variations of surface forces and how they change with the wave wavenumber are going to be observed in the following. Results presented in Fig. 4.3 (a) illustrate:

- how the x -component of the pressure force acting on the fluid at the lower wall wave varies over one wavelength,
- how this distribution changes with the change of the wavenumber,
- that $\sigma_{xp,L}$ increases with the increase of the wave number i.e., as the wavenumber increases, $\sigma_{xp,L}$ increases causing a more intense movement of the fluid.

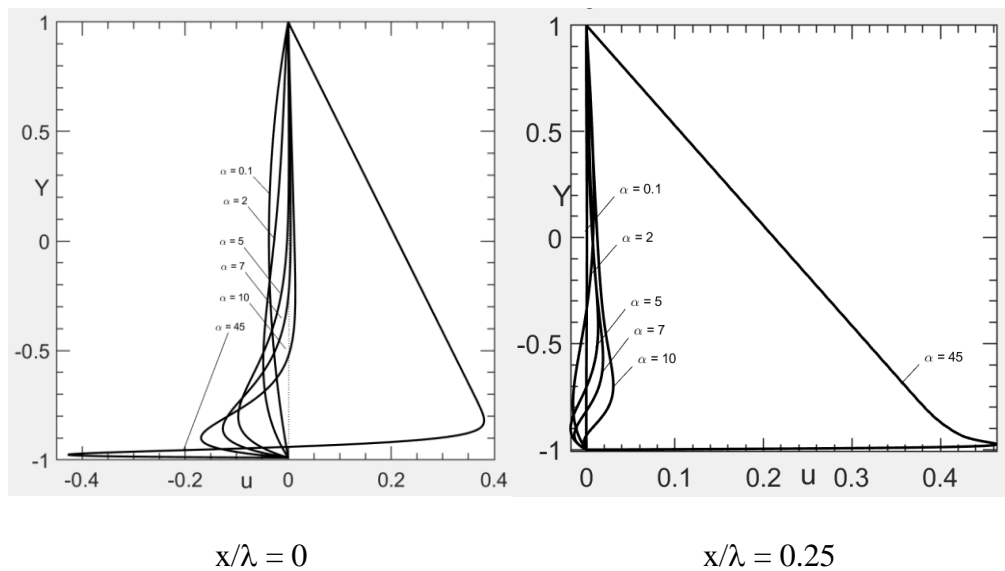
Results presented in Fig. 4.3 (b) illustrate:

- how the x -component of the viscous force acting on the fluid at the lower wall varies over one wavelength,
- how its distribution changes with the change of the wavenumber,
- that the magnitude of $\sigma_{xv,L}$ increases with an increase of the wavenumber i.e., $\sigma_{xv,L}$ generates bigger resistance to the fluid movement as the wavenumber increases.

Results presented in Fig 4.3 (c) illustrate:

- how the x -component of the viscous force acting on fluid at the upper wall varies over one wavelength,
- how its distribution changes with the change of the wavenumber,
- that the magnitude of $\sigma_{xv,U}$ increases with an increase of the wavenumber i.e., $\sigma_{xv,U}$ generates bigger resistance to the fluid movement as the wavenumber increases.

Figure 4.4 illustrates velocity profiles at different locations of the wave. It can be seen that fluid changes direction of its movement depending on its position with respect to the wave. The character of these changes varies with the wave wavenumber. At small wavenumbers, the forward/backward movement extends across the conduit creating “sloshing” which produces a small net forward movement. As α increases, this “sloshing” is confined to a progressively smaller zone attached to the vibrating wall while the net forward movement increases. Figure 4.5 displays the same velocity profiles but grouped according to the wave wavenumbers. The “sloshing” effect along the wave wavelength is well illustrated and its progressive confinement closer and closer to the vibrating wall as α increases is well underlined.



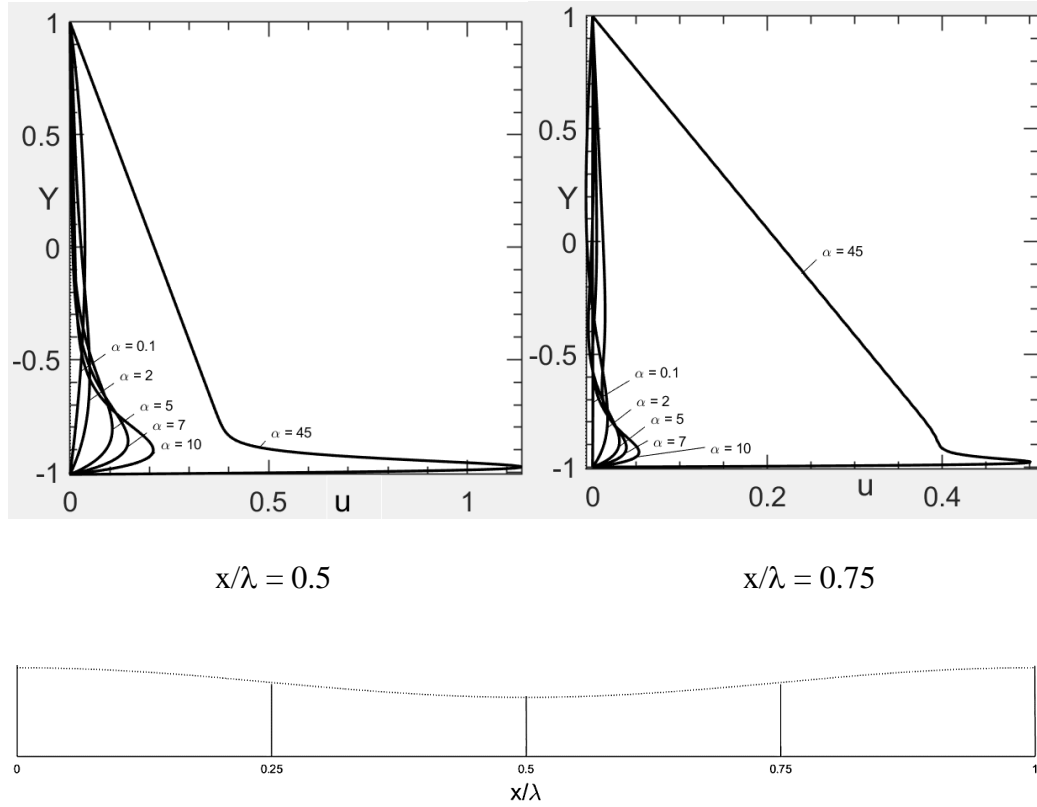
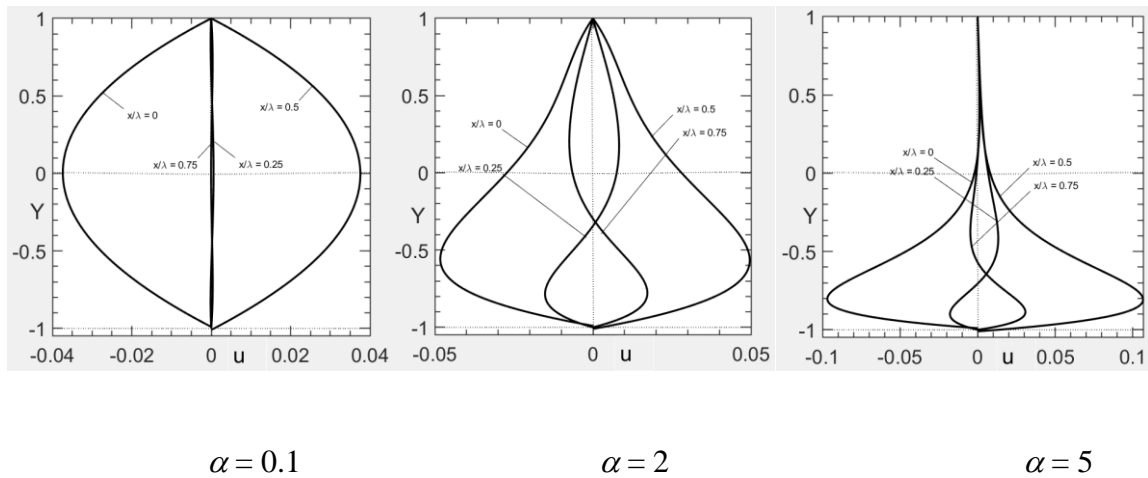


Figure 4.4: u -velocity profiles at selected locations. At each location, the variation of the u -velocity profile is shown for selected wavenumbers. Computations are carried out for the amplitude $A = 0.01$ and the wave phase speed $c = 5$.



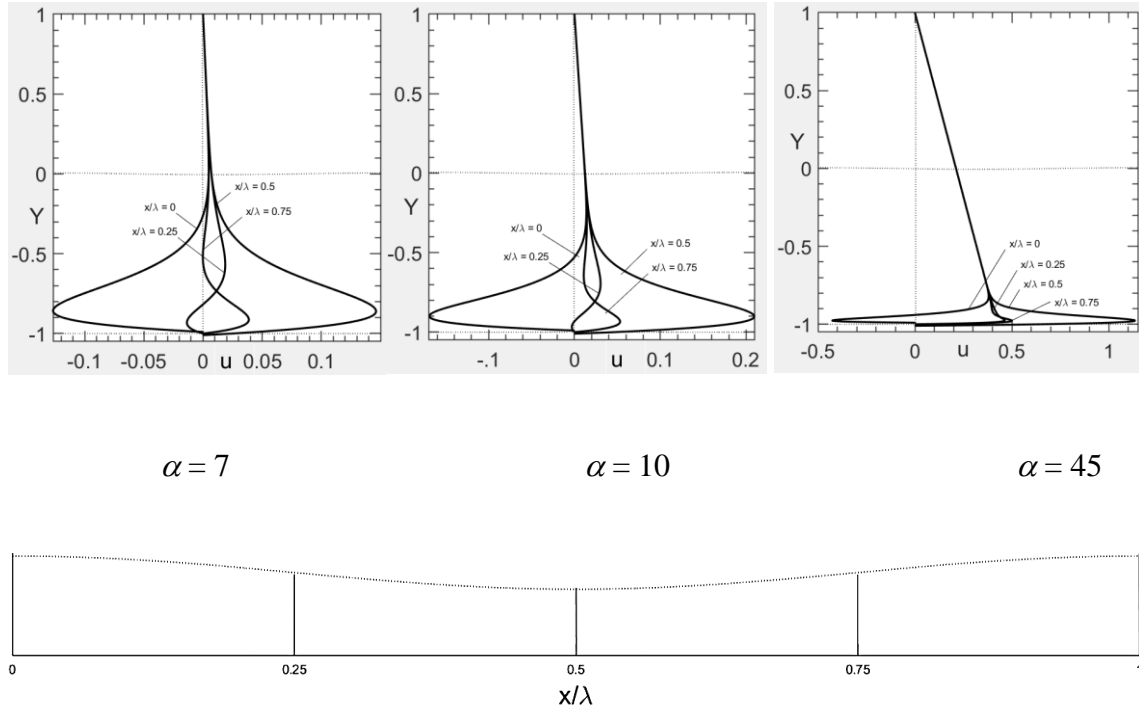


Figure 4.5 u -velocity profiles for selected wavenumbers. At each wavenumber, the variation of the u -velocity profile is shown at four different locations. Computations are carried out for the wave amplitude $A = 0.01$ and the wave phase speed $c = 5$.

The character of the fluid movement is illustrated in Fig. 4.6 displaying instantaneous vector lines over one wave wavelength. Large zones of backward moving fluid are found for waves with small wavenumbers. A typical particle would undergo large amplitude forward/backward movements with a small preference for the forward movement. The flow separation zones decrease with an increase of α until the sloshing is confined to a very narrow layer adjacent to the vibrating wall with most of the fluid moving to the right in a nearly rectilinear manner.

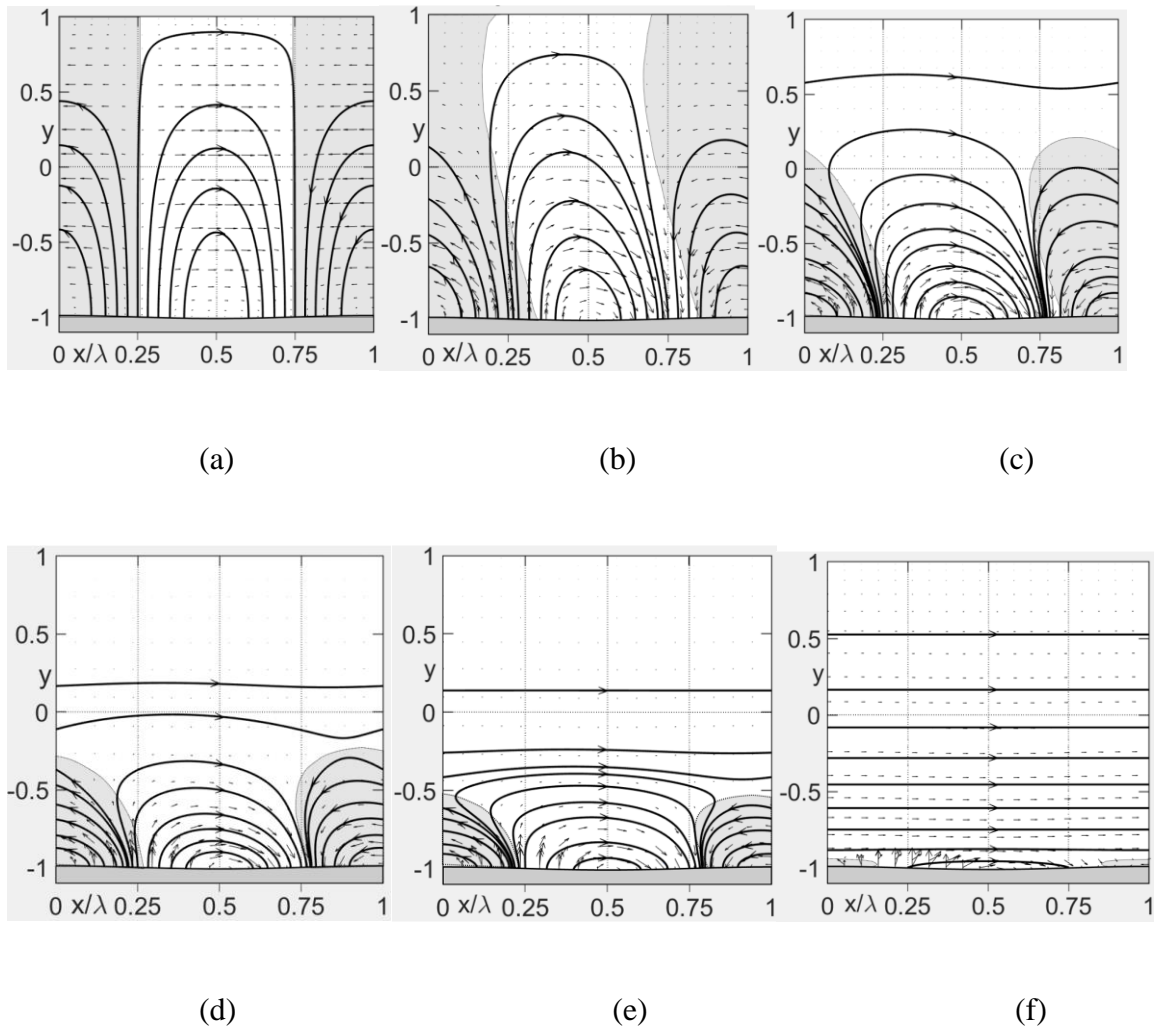


Figure 4.6 Plots of velocity fields. (a) to (f) correspond to $\alpha = 0.1, 2, 5, 7, 10, 45$, respectively, for the wave phase speed $c = 5$ and the wave amplitude $A = 0.01$. Flow zones with fluid moving in the opposite direction are identified using shading.

4.2 Effect of variations of the wave amplitude

Variations of the flow rate Q with the wave amplitude A are illustrated in Fig. 4.7. It can be seen that Q increases proportionally to A^2 in the whole range of wavenumbers in the range of A being of interest in this analysis.

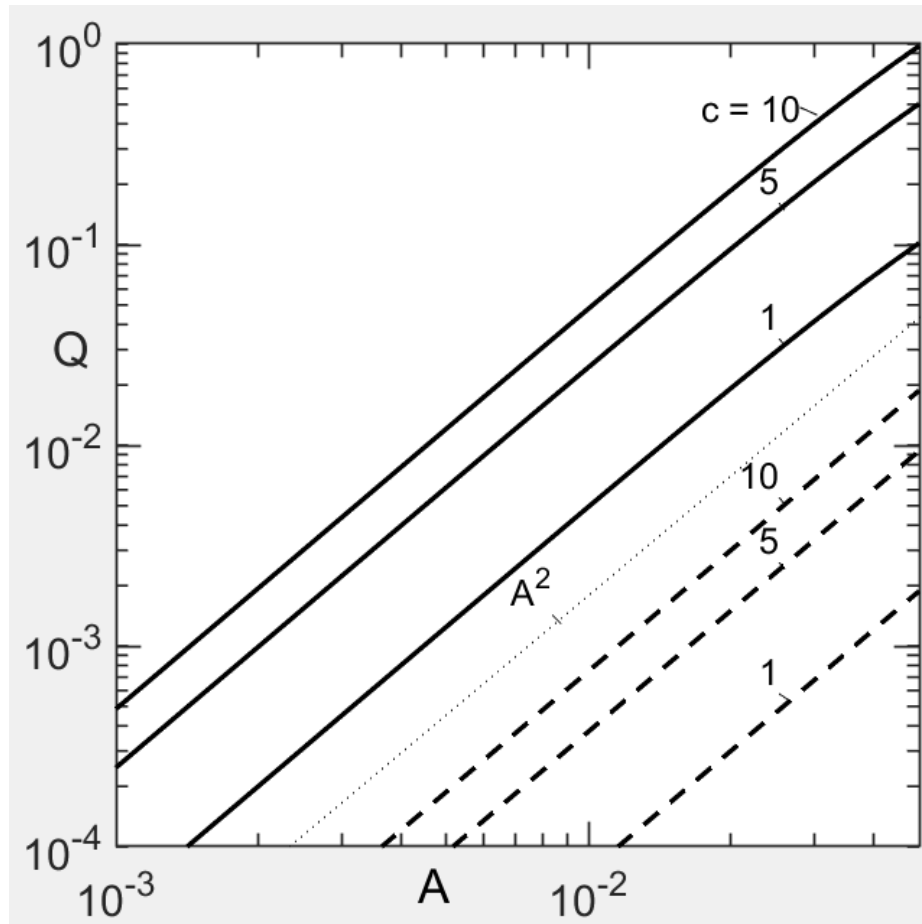


Figure 4.7 Plots of variations of the flow rate Q as a function of the wave amplitude A for selected wave phase speeds $c = 1, 5, 10$. Dashed lines correspond to the wavenumber $\alpha = 0.1$ and solid lines correspond to the wavenumber $\alpha = 10$.

4.3 Effect of variations of the wave phase speed

Variations of the flow rate Q with the wave phase speed are illustrated in Fig. 4.8. It can be seen that Q increases proportionally to c in the whole range of wavenumbers being of interest in this analysis.

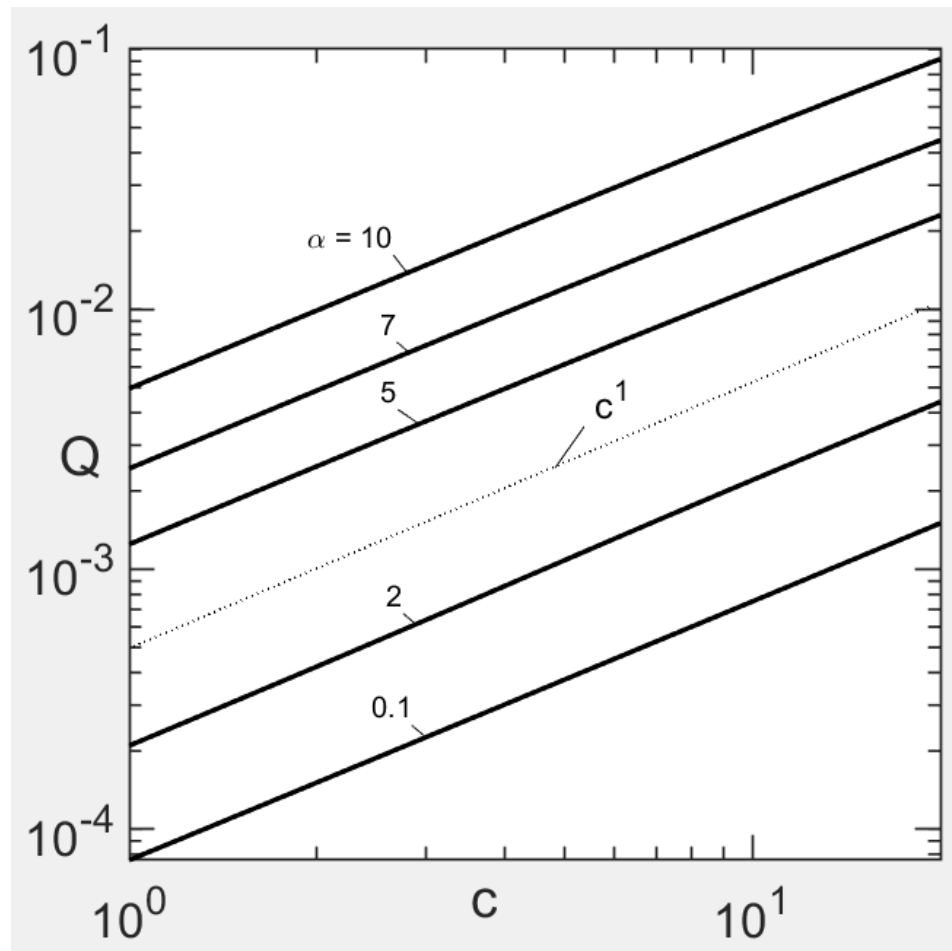


Figure 4.8 Plots of variations of the flow rate Q as a function of the wave phase speed c for selected wavenumbers ($\alpha = 0.1, 2, 5, 7, 10$)

4.4 Effect of the phase difference

The effect of the relative positions of the upper and lower waves as quantified by the phase shift Ω is going to be discussed in this section. Amplitudes of both waves are set to be the same and equal to A . Results displayed in Fig.4.9 demonstrate large sensitivity of the flow rate to variations of Ω as long as the wave wavenumber is small enough. Under such conditions, the largest flow rate is achieved when the phase difference corresponds to half of the wave wavelength. It has been shown previously that fluid movement involves large forward/backward “sloshing” with a small net forward movement. This “sloshing” is strongly affected by the relative position of both waves. As the wavenumber increases, “sloshing” is confined to thinner and thinner zones adjacent to vibrating walls, and the flow

losses sensitivity to variations of the phase difference. Each “sloshing” zone acts independently from the other with the fluid moving in a nearly rectilinear manner in the central zone of the conduit. A significant increase in the flow rate (when compared with the one wall vibrations) is achieved under such conditions.

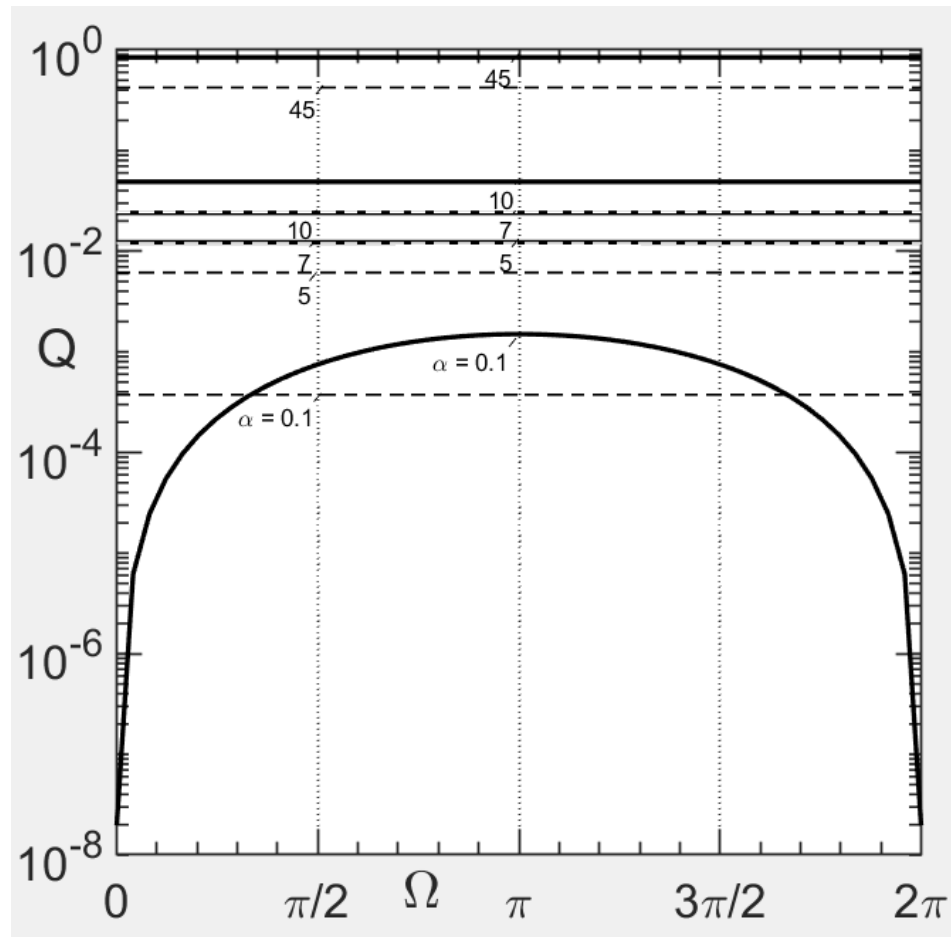


Figure 4.9 Plots of variations of the flow rate Q as a function of the phase difference Ω between the waves at the upper and lower walls for the phase speed $c = 5$ and the amplitude $A = 0.01$ for selected wavenumbers. Dashed lines indicate results for the one-wall vibrations.

Chapter 5

5 Conclusions and Recommendations

5.1 Conclusions

This thesis presents a grid-less, spectrally accurate algorithm for analyzing flows through channels with moving boundaries. It uses a fixed regular computational domain where the boundary conditions were expressed as internal constraints. It is capable of simulating waves of arbitrary shapes. The presence of the waves results in an irregular solution domain and hence, necessitates the use of proper solution methodologies capable to deal with the irregular flow domains. The algorithm uses the Immersed Boundary Conditions (IBC) concept. This eliminates the need for a costly numerical coordinate generation while permitting the use of a simple computational domain. It employs Fourier expansions in the streamwise direction and Chebyshev expansions in the cross-flow direction. This algorithm is very flexible from the point of view of the analysis of waves with various shapes as long as these shapes can be described by Fourier expansions. The field equations are discretized using a regular, rectangular computational domain with the flow domain with moving boundaries immersed inside the computational domain. Galerkin procedure is used to construct the relevant algebraic equations. Boundary conditions are included in the discretized problem using the Tau procedure. These conditions are expressed in terms of Fourier expansions based on the shape of the moving boundaries to make them suitable for inclusion in the algorithm. The solution procedure employs the iterative process with the nonlinear terms taken from the previous iteration. This results in the first-order fixed-point method.

Investigations of flow properties were carried out for vibrations applied either at a single wall or on both walls. For the case of the one-wall vibrations, the effects of the wave wavenumbers, the amplitude, and the phase speed were investigated whereas, for the case of the two-wall vibrations, the effect of the phase difference between the upper and lower waves were included in the investigation. In all these cases, the effectiveness of vibrations was assessed by determining the flow rate generated by these vibrations.

The results show the dependence of the flow rate on the wave wavenumber. It was found that the variations of the flow rate follow asymptotes at the two extreme cases i.e., for very small wavenumber and very large wavenumber. The flow rate remains nearly constant when the wavenumber increases but starts to increase rapidly once the wavenumber increases beyond unity. At higher wavenumbers, the flow rate increases proportionally to $\alpha^{1.73}$. Analysis of viscous and pressure forces acting on the fluid at the walls shows that the fluid movement is driven by the pressure force generated at the vibrating wall and is opposed by the viscous friction. It was observed that the flow rate increased proportionally to the second power of the wave amplitude and proportionally to the first power of the wave phase speed. It was further observed that the variations of the flow rate with the phase difference between the waves at the upper and lower walls were symmetric about the relative position corresponding to the half of the wave wavelength, and this relative position of the waves generated the highest flow rate.

Only waves with sinusoidal shape were investigated in this thesis.

5.2 Recommendations for future work

As only the sinusoidal waves were considered in this thesis, further investigations could look at different wave shapes and could determine the optimal wave shape, i.e. shape which produces the largest flow rate. The analysis could extend to the determination of the system response to the commensurable and non-commensurable wave shapes.

One may find it to be of interest to investigate other effects combined with the peristaltic effect, e.g. combination of the wall transpiration with the peristaltic effect, combination of heating patterns applied at the walls with the peristaltic effect, etc.

A similar investigation can be extended to non-Newtonian fluids after making the necessary adjustments to the algorithm.

References

- Kim, Eui-Gyu and Oh, Jae-geun and Choi, Bumkyoo. (2006). A study on the development of a continuous peristaltic micropump using magnetic fluids. *Sensors and Actuators A: Physical*. 128. 43-51. 10.1016/j.sna.2006.01.021.
- Neto, A. and Lima, Antonio and Neff, Helmut and Gomes, Caio and Moreira, Cleumar. (2011). Linear peristaltic pump driven by three magnetic actuators: Simulation and experimental results. *Conference Record - IEEE Instrumentation and Measurement Technology Conference*. 1-6. 10.1109/IMTC.2011.5944300.
- Al-Halhouli, Ala'aldeen, and Kilani, Mohammad, and Büttgenbach, Stephanus. (2010). Development of a novel electromagnetic pump for biomedical applications. *Sensors and Actuators A: Physical*. 162. 172-176. 10.1016/j.sna.2010.02.001.
- Abd elnaby, Abd elhakeem, and Misiery, A. E. M. (2002). Effects of an endoscope and generalized Newtonian fluid on peristaltic motion. *Applied Mathematics and Computation*. 128. 19-35. 10.1016/S0096-3003(01)00153-9.
- Abd elnaby, abd elhakeem. (2004). Effects of an endoscope and fluid with variable viscosity on peristaltic motion. *Applied Mathematics and Computation*. 158. 497–511.
- Hayat, Tasawar, and Momoniat, E., and Mahomed, F. (2006). Endoscope effects on MHD Peristaltic flow of power law fluid. *Mathematical Problems in Engineering*. 2006. 10.1155/MPE/2006/84276.

- Khan, A. and Sohail, Dr Ayesha and Rashid, Sadia, and Khan, Najeeb. (2015). Effects of slip condition, variable viscosity, and inclined magnetic field on the peristaltic motion of a non-Newtonian fluid in an inclined asymmetric channel. *Journal of Applied Fluid Mechanics*. 9.
- Tripathi, Dharmendra, and Chaube, M., and Gupta, Praveen. (2011). Stokes flow of micropolar fluids by peristaltic pumping through the tube with slip boundary condition. *Applied Mathematics and Mechanics*. 32. 10.1007/s10483-011-1525-6.
- Tripathi, Dharmendra. (2011). A mathematical model for the peristaltic flow of chyme movement in the small intestine. *Mathematical biosciences*. 233. 90-7. 10.1016/j.mbs.2011.06.007.
- Tripathi, Dharmendra, and Pandey, S, and Das, S. (2011). Peristaltic transport of a generalized Burgers' fluid: Application to the movement of chyme in the small intestine. *Acta Astronautica - ACTA ASTRONAUT*. 69. 30-38. 10.1016/j.actaastro.2010.12.010.
- Tripathi, Dharmendra, and Bég, O. (2012). Magnetohydrodynamic peristaltic flow of a couple stress fluid through coaxial channels containing a porous medium. *Journal of Mechanics in Medicine and Biology*. 12. 10.1142/S0219519412500881.
- Tripathi, Dharmendra. (2012). Peristaltic Hemodynamic Flow of Couple-Stress Fluids Through a Porous Medium with Slip Effect. *Transport in Porous Media*. 10.1007/s11242-011-9920-9.
- Tripathi, Dharmendra, and Bég, O., and Pandey, Vinay, and Singh, A. K. (2013). A Study of Creeping Sinusoidal Flow of Bio-Rheological Fluids through a Two-Dimensional High Permeability Medium Channel. *Journal of Advanced Biotechnology and Bioengineering*. 1. 52-61. 10.12970/2311-1755.2013.01.02.2.
- Kothandapani, M., and Jayavel, Prakash. (2014). The peristaltic transport of Carreau Nanofluids under effect of a magnetic field in a tapered asymmetric channel: Application of the cancer therapy. *Journal of Mechanics in Medicine and Biology*. 15. 1550030. 10.1142/S021951941550030X.
- Kothandapani, M., and Jayavel, Prakash. (2015). Effects of thermal radiation parameter and magnetic field on the peristaltic motion of Williamson nanofluids in a tapered asymmetric channel. *International Journal of Heat and Mass Transfer*. 81. 10.1016/j.ijheatmasstransfer.2014.09.062.
- Akbar, Noreen, and Butt, Adil. (2016). Ferromagnetic effects for peristaltic flow of Cu-water nanofluid for different shapes of nano-size particles. *Applied Nanoscience*. 6. 379-385. 10.1007/s13204-015-0430-x.
- Kumari, A. and G. Radhakrishnamacharya, (2012). Effect of slip and magnetic field on peristaltic flow in an inclined channel with wall effects. *International Journal of Biomathematics*. 05. 10.1142/S1793524511001568.
- Ramesh, Dr, and Devakar, M. (2018). Effect of endoscope on the peristaltic transport of a couple stress fluid with heat transfer: Application to biomedicine. *Nonlinear Engineering*. 8. 10.1515/nleng-2017-0166.

- Ellahi, Rahmat, and Hussain, Farooq. (2015). Simultaneous effects of MHD and partial slip on peristaltic flow of Jeffery fluid in a rectangular duct. 10.1016/j.jmmm.2015.05.04.
- Ellahi, Rahmat and Hassan, Mohsan, and Zeeshan, Ahmad. (2015). Study of Natural Convection MHD Nanofluid by Means of Single and Multi-Walled Carbon Nanotubes Suspended in a Salt-Water Solution. IEEE Transactions on Nanotechnology. 14. 1-1. 10.1109/TNANO.2015.2435899.
- Sheikholeslami, M., and Ellahi, Rahmat. (2015). Three-dimensional mesoscopic simulation of magnetic field effect on natural convection of nanofluid. International Journal of Heat and Mass Transfer. 89. 799-808. 10.1016/j.ijheatmasstransfer.2015.05.110.
- Shehawey, Elsayed, and Sebaei, Wahed. (2000). Peristaltic transport in a cylindrical tube through a porous medium. International Journal of Mathematics and Mathematical Sciences. 24. 10.1155/S0161171200004737.
- Hayat, Tasawar and Ali, Niaz and Asghar, Saleem. (2007). Effects on peristaltic flow of a Maxwell fluid in a porous medium. Physics Letters A - PHYS LETT A. 363. 397-403. 10.1016/j.physleta.2006.10.104.
- Vajravelu, Kuppapalle, and Radhakrishnamacharya, G., and Radhakrishnamurthy, V. (2007). Peristaltic flow and heat transfer in a vertical porous annulus, with long-wave approximation. International Journal of Non-Linear Mechanics. 42. 754-759. 10.1016/j.ijnonlinmec.2007.02.014.
- Dr, C Vasudev, and Rao, (2010). Peristaltic Pumping of Williamson fluid through a porous medium in a horizontal channel with heat transfer. American Journal of Scientific and Industrial Research. 1. 656-666. 10.5251/ajsir.2010.1.3.656.666.
- Tripathi, Dharmendra, and Bég, O. (2012). A Numerical Study of Oscillating Peristaltic Flow of Generalized Maxwell Viscoelastic Fluids Through a Porous Medium. Transport in Porous Media. 95. 10.1007/s11242-012-0046-5.
- Prasad, Pothukuchi and Gupta, Shivani and Sreeramulu, M. and Sundar, L. and Singh, Manoj, and Sousa, Antonio. (2015). Experimental study of heat transfer and friction factor of Al₂O₃ nanofluid in U-tube heat exchanger with helical tape inserts. Experimental Thermal and Fluid Science. 62. 10.1016/j.expthermflusci.2014.12.006.
- Prasad, V. Ramachandra, and Gaffar, S., and Bég, O. (2014). Heat and Mass Transfer of Nanofluid from Horizontal Cylinder to Micropolar Fluid. Journal of Thermophysics and Heat Transfer. 29. 1-13. 10.2514/1.T4396.
- Lu, Lin, and Liu, ZHEN-HUA, and Xiao, Hong-Sheng. (2011). Thermal performance of an open thermosyphon using nanofluids for high temperature evacuated tubular solar collectors Part 1: Indoor experiment. Solar Energy - SOLAR ENERGY. 85. 379-387. 10.1016/j.solener.2010.11.008.
- Hayat, T., Ahmed, B., Abbasi, F.M. et al. (2019) Peristalsis of nanofluid through a curved channel with Hall and Ohmic heating effects. J. Cent. South Univ. 26, 2543–2553. <https://doi.org/10.1007/s11771-019-4193-5>

- Jayavel, Prakash and Parthasarathy, Siva and Tripathi, Dharmendra, and Kothandapani, M. (2019). Nanofluids flow driven by peristaltic pumping in the occurrence of magnetohydrodynamics and thermal radiation. *Materials Science in Semiconductor Processing*. 100. 290-300. 10.1016/j.mssp.2019.05.017.
- Hayat, T. and Ahmed, Bilal and Abbasi, F. and Alsaedi, Ahmed. (2017). Hydromagnetic peristalsis of water-based nanofluids with temperature-dependent viscosity: A comparative study. *Journal of Molecular Liquids*. 234. 324-329. 10.1016/j.molliq.2017.03.080.
- Khaled, S. M., and Ebaid, Abdelhalim, and Mutairi, Fahd. (2014). The Exact Endoscopic Effect on the Peristaltic Flow of a Nanofluid. *Journal of Applied Mathematics*. 2014. 10.1155/2014/367526.
- Ebaid, Abdelhalim, and Aly, Emad. (2013). Exact Analytical Solution of the Peristaltic Nanofluids Flow in an Asymmetric Channel with Flexible Walls and Slip Condition: Application to the Cancer Treatment. *Computational and mathematical methods in medicine*. 2013. 825376. 10.1155/2013/825376.
- Tripathi, Dharmendra, and Béq, O. (2014). A study on the peristaltic flow of nanofluids: Application in drug delivery systems. *International Journal of Heat and Mass Transfer*. 70. 61–70. 10.1016/j.ijheatmasstransfer.2013.10.044.
- Jayavel, Prakash and Tripathi, Dharmendra and Tiwari, Abhishek and Sait, Sadiq, and Ellahi, Rahmat. (2019). Peristaltic Pumping of Nanofluids through a Tapered Channel in a Porous Environment: Applications in Blood Flow. *Symmetry*. 11. 868. 10.3390/sym11070868.
- Akbar, Noreen, and Hayat, Tasawar and Nadeem, Prof. Dr. Sohail, and Obaidat, Saleem. (2012). Peristaltic flow of a Williamson fluid in an inclined asymmetric channel with partial slip and heat transfer. *International Journal of Heat and Mass Transfer*. 55. 1855–1862. 10.1016/j.ijheatmasstransfer.2011.11.038.
- Mustafa, Meraj and Hina, Sadia and Hayat, Tasawar and Ahmad, Bashir. (2014). Influence of induced magnetic field on the peristaltic flow of nanofluid. *Meccanica*. 3. 10.1007/s11012-013-9809-5.
- Akbar, Noreen, and Nadeem, Prof. Dr. Sohail and Hayat, Tasawar and Hendi, Awatif. (2012). Peristaltic flow of a nanofluid with slip effects. *Meccanica*. 47. 10.1007/s11012-011-9512-3.
- Aly, Emad, and Ebaid, Abdelhalim. (2014). Effect of the Velocity Second Slip Boundary Condition on the Peristaltic Flow of Nanofluids in an Asymmetric Channel: Exact Solution. *Abstract and Applied Analysis*. 2014. 1-11. 10.1155/2014/191876.
- Kumar, S Ravi. (2010). Peristaltic flow of a couple stress fluid in a flexible channel under an oscillatory flux. *Int. J. of Appl. Math and Mech*. 6. 58-71.
- Ali, Nasir, and Hayat, Tasawar, and Sajid, M. (2007). Peristaltic flow of a Couple stress fluid in an asymmetric channel. *Biorheology*. 44. 125-38.

- Eldabe, Nabil and Elshaboury, Samy and Hasan, Alfaisal, and Elogail, M. (2012). MHD Peristaltic Flow of a Couple Stress Fluids with Heat and Mass Transfer through a Porous Medium. *Innov. Syst. Des. Eng.* 3.
- Swarnalathamma, B., and Krishna, M. Veera. (2016). Peristaltic hemodynamic flow of couple stress fluid through a porous medium under the influence of magnetic field with slip effect. 1728. 020603. 10.1063/1.4946654.
- Hummady, Lika and Abdulhadi, Ahmed and Hummudy, Liqaa. (2014). Influence of MHD on Peristaltic Flow of Couple-Stress Fluid Through a Porous Medium with Slip Effect. 30,2014. 34-48.
- Alsaedi, A. and Ali, Nasir and Tripathi, Dharmendra and Hayat, Tasawar. (2014). Peristaltic flow of couple stress fluid through uniform porous medium. *Applied Mathematics and Mechanics.* 35. 469-480. 10.1007/s10483-014-1805-8.
- Mekheimer, Kh. (2002). Peristaltic flow of a couple stress fluid in a uniform and non-uniform channel. *Biorheology.* 39. 755-65.
- Hina, Sadia, and Mustafa, Meraj, and Hayat, Tasawar. (2015). On the exact solution for peristaltic flow of couple-stress fluid with wall properties. *Izvestiya po Khimiya Bulgarska Akademiya na Naukite.* 47. 30-37.
- Hina, Sadia, and Mustafa, Meraj and Hayat, Tasawar, and Al Saedi, A. (2015). Peristaltic flow of couple-stress fluid with heat and mass transfer: An application in biomedicine. *Journal of Mechanics in Medicine and Biology.* 15. 1550042. 10.1142/S0219519415500426.
- Kumar, S Ravi. (2015). Effect of Couple Stress Fluid Flow on Magnetohydrodynamic Peristaltic Blood Flow with Porous Medium through Inclined Channel in the Presence of Slip Effect - Blood Flow Model. *International Journal of Bioscience and Bio-Technology.* 7. 65-84. 10.14257/ijbsbt.2015.7.5.07.
- Vidhya, Mohanakrishnan, and Parthasarathy, Siva, and Govindarajan, A. (2015). MHD peristaltic flow of a couple stress fluids permeated with suspended particles through a porous medium under long wavelength approximation. *ARPN Journal of Engineering and Applied Sciences.* 10. 3072-3077.
- Elmaboud, Y. and Mekheimer, Kh, and Abdellateef, A.I. (2013). Thermal Properties of Couple-Stress Fluid Flow in an Asymmetric Channel with Peristalsis. *Journal of Heat Transfer.* 135. 10.1115/1.4023127.
- Kumar, P, and Kavitha, A, and R., Saravana. (2017). Hall effects on peristaltic flow of couple stress fluid in a vertical asymmetric channel. *IOP Conference Series: Materials Science and Engineering.* 263. 062021. 10.1088/1757-899X/263/6/062021.
- Tsiklauri, David, and Beresnev, Igor. (2001). Non-Newtonian effects in the peristaltic flow of a Maxwell fluid. *Physical review. E, Statistical, nonlinear, and soft matter physics.* 64. 036303. 10.1103/PhysRevE.64.036303.

- El-Shehawey, E. and El-Dabe, N. and Eldesoky, Islam. (2006). Slip effects on the peristaltic flow of a non-Newtonian Maxwellian fluid. *Acta Mechanica*. 186. 141-159. 10.1007/s00707-006-0343-6.
- Eldabe, Nabil and Ghaly, A.Y. and Sayed, Haneen. (2007). MHD peristaltic flow of non-Newtonian fluid through a porous medium in circular cylindrical tube. *Bulletin of the Calcutta Mathematical Society*. 99.
- Hayat, Tasawar and Khan, M. and Siddiqui, Abdul, and Asghar, Saleem. (2007). Non-linear peristaltic flow of a non-Newtonian fluid under the effect of a magnetic field in a planar channel. *Communications in Nonlinear Science and Numerical Simulation*. 12. 910-919. 10.1016/j.cnsns.2005.08.007.
- Ali, Nasir, and Sajid, M. and Abbas, Z. and Javed, Tabish. (2010). Non-Newtonian fluid flow induced by peristaltic waves in a curved channel. *European Journal of Mechanics - B/Fluids*. 29. 387-394. 10.1016/j.euromechflu.2010.04.002.
- Kalantari, Alireza, and Sadeghy, Kayvan, and Sadeqi, S. (2013). Peristaltic flow of non-Newtonian fluids through curved channels: A numerical study. *Annu. Trans. Nord. Rheol. Soc*. 21. 163-170.
- Maiti, s and Misra, J. (2011). Non-Newtonian characteristics of peristaltic flow of blood in micro-vessels. *Communications in Nonlinear Science and Numerical Simulation*. 18. 10.1016/j.cnsns.2012.12.015.
- Mekheimer, Kh, and Abdel-Wahab, A.N. (2013). Compressibility effects on peristaltic flow of a non-Newtonian Maxwell fluid through an annulus. *Fluid Transport: Theory, Dynamics and Applications*. 219-236.
- Hina, Sadia, and Mustafa, Meraj and Hayat, Tasawar, and Alsaedi, A. (2013). Peristaltic Flow of Pseudoplastic Fluid in a Curved Channel with Wall Properties. *Journal of Applied Mechanics*. 80. 4501-.10.1115/1.4007433.
- Javed, Maryiam, and Hayat, Tasawar, and Alsaedi, A. (2014). Effect of Wall Properties on the Peristaltic Flow of a Non-Newtonian Fluid. *Applied Bionics and Biomechanics*. 11. 207-219. 10.1155/2014/802361
- Hayat, Tasawar and Yasmin, Humaira, and Alsaedi, A..(2014). Convective heat transfer analysis for peristaltic flow of power-law fluid in a channel. *Journal of the Brazilian Society of Mechanical Sciences and Engineering*. 37. 10.1007/s40430-014-0177-4.
- Ellahi, Rahmat and Rahman, S. and Gulzar, M. and Nadeem, Prof. Dr. Sohail and Vafai, Kambiz. (2014). A Mathematical Study of Non-Newtonian Micropolar Fluid in Arterial Blood Flow Through Composite Stenosis. *Applied Mathematics and Information Sciences*. 8. 1567-1573. 10.12785/amis/080410.
- Singh, Udaya. (2016). An Exact Solution of Non-Newtonian Peristaltic Flow in a Tube : Rabinowitsch Fluid Model. *Journal of Science of the University of Kelaniya Sri Lanka*. 10. 1.10.4038/josuk.v10i0.7991.
- Singh, Udaya and Medhavi, Amit and Gupta, R.S. and Bhatt, Siddharth. (2017). Analysis of Peristaltic Transport of Non-Newtonian Fluids Through Nonuniform Tubes:

- Rabinowitsch Fluid Model. *Zeitschrift für Naturforschung A*. 72. 10.1515/zna-2017-0033.
- Alokaily, Samer. (2017). Master's thesis. Modeling and simulation of the peristaltic flow of Newtonian and non-Newtonian fluids with application to the human body.
- Kumar, Thanesh, and Kavitha, A., and R., Saravana. (2018). Peristaltic flow of an Ellis fluid model in an inclined uniform tube with wall properties. *International Journal of Mechanical Engineering and Technology*. 9. 15-27.
- Vaidya, Hanumesh and Choudhari, Rajashekhar and Gudekote, Manjunatha and Prasad, Kerehalli and Makinde, Oluwole, and Sreenadh, S. (2019). Peristaltic Motion of Non-Newtonian Fluid with Variable Liquid Properties in a Convectively Heated Non-Uniform Tube: Rabinowitsch Fluid Model. *Journal of Enhanced Heat Transfer*. 26. 10.1615/JEnhHeatTransf.2019029230.
- Meyer, G, and Gernhardt, D and Castell, D. (2000). Peristaltic Pressure Profiles of the Human Esophagus. *Journal of clinical gastroenterology*. 30. 270-3. 10.1097/00004836-200004000-00013.
- Allen, M., and Zamani, S., and Jr, A. (2003). The effect of gravity on oesophageal peristalsis in humans. *Neurogastroenterology and Motility*. 9. 71 - 76. 10.1046/j.1365-2982.1997.d01-19.x.
- Watanabe, Makoto and Sekine, Kazumitsu and Hori, Yoshio and Shiraishi, Yasuyuki and Maeda, Takeshi and Honma, Dai and Miyata, Go and Saijo, Yoshifumi and Yambe, Tomoyuki. (2005). Artificial Esophagus with Peristaltic Movement. *ASAIO journal (American Society for Artificial Internal Organs: 1992)*. 51. 158-61. 10.1097/01.MAT.0000154644.44891.F1.
- Teran, Joseph, and Fauci, Lisa, and Shelley, Michael. (2006). Large-Amplitude Peristaltic Pumping of a Viscoelastic Fluid.
- Miki, Hiroyuki, and Okuyama, Takeshi and Kodaira, Shingo and Luo, Yun and Takagi, Toshiyuki, and Yambe, Tomoyuki. (2010). Property evaluation of an artificial esophagus with peristaltic motion using shape memory alloy. *Nihon Kikai Gakkai Ronbunshu, C Hen/Transactions of the Japan Society of Mechanical Engineers, Part C*. 76. 1560-1566. 10.3233/JAE-2010-1176.
- Suzuki, Kazuyuki, and Nakamura, Taro. (2010). Development of a Peristaltic Pump Based on Bowel Peristalsis using Artificial Rubber Muscle. *Advanced Robotics*. 25. 3085 - 3090. 10.1109/IROS.2010.5653006.
- Walker, Shawn, and Shelley, Michael. (2010). Shape optimization of peristaltic pumping. *J. Comput. Physics*. 229. 1260-1291. 10.1016/j.jcp.2009.10.030.
- Toklu, Ethem. (2011). A new mathematical model of peristaltic flow on esophageal bolus transport. *Scientific Research and Essays*. 6. 10.5897/SRE11.1502.
- Misra, J. and Maiti, s. (2011). Peristaltic Transport of a Rheological Fluid: Model for Movement of Food Bolus Through Esophagus. *Applied Mathematics and Mechanics*. 33. 10.1007/s10483-012-1552-7.

- Dirven, Steven and Chen, F.J. and Xu, Peter and Bronlund, John and Allen, Jacqueline and Cheng, Leo. (2014). Design and Characterization of a Peristaltic Actuator Inspired by Esophageal Swallowing. *Mechatronics, IEEE/ASME Transactions on*. 19. 1234-1242. 10.1109/TMECH.2013.2276406.
- Dirven, Steven, and Xu, Peter, and Cheng, Leo. (2014). Sinusoidal Peristaltic Waves in Soft Actuator for Mimicry of Esophageal Swallowing. *IEEE/ASME Transactions on Mechatronics*. 20. 1-7. 10.1109/TMECH.2014.2337291.
- Esser, Falk and Krüger, Friederike and Masselter, Tom and Speck, Thomas. (2019). Characterization of biomimetic peristaltic pumping system based on flexible silicone soft robotic actuators as an alternative for technical pumps.
- Croce, G. and D'Agaro, P., 2005, Numerical simulation of roughness effect on microchannel heat transfer and pressure drop in laminar flow, *J. Phys. D: Appl. Phys.*, vol. 38, pp. 1518-1530.
- Yoon, S., Na, S., Wang, Z.J., Bons, J.P. and Shih, T.I-P. 2006 Flow and heat transfer over rough surfaces: usefulness of 2-D roughness-resolved simulations, *44' Aero. Sci. Meet. Exhibit*, Reno, Nevada.
- Jiang, Y. and Floryan, J.M., 2005 Finite-difference 4th-order compact scheme for the direct numerical simulation of instabilities of shear layers, *Int. J. Numer. Meth. Fluids*, vol. 48, pp. 1259-1281
- Husain, S.Z. and Floryan, J.M., 2007 Immersed boundary conditions method for unsteady flow problems described by the Laplace operator, *Int. J. Num. Meth. Fluids*, vol. 56, pp. 1765-1786.
- Tsangaris, S. and Potamitis, D., 1986 On laminar small Reynolds-number flow over wavy walls, *Acta Mechanica*, vol. 61, pp. 109-115
- Cabal T., Szumbariski J., and Floryan J.M., 2002 Stability of flow in a wavy channel, *J. Fluid Mech.*, **457**, 191.
- Mittal, R. and Iaccarino, G., 2005 Immersed boundary methods, *Annu. Rev. Fluid Mech.*, vol. 37 pp. 239-261
- Szumbariski J. and Floryan J. M., 1999 "A direct spectral method for determination of flows over corrugated boundaries," *J. Comp. Phys.* 153, 378-402.
- Canuto, C, Hussaini, M.Y., Quarteroni, A., and Zang, T.A., 1987 Spectral methods in fluid dynamics, *Springer*

Appendices

Appendix A: Evaluation of Fourier Expansion of Chebyshev Polynomials and their derivatives

This section will describe how to derive Fourier expansions of Chebyshev polynomials and their derivatives along the upper wall.

Evaluation of Fourier Expansion of Chebyshev Polynomials

This sub-section will show how to derive Fourier expansions of Chebyshev polynomials.

Let, the Fourier expansion of Chebyshev polynomial T_k along the upper wall is given by:

$$T_k(\hat{y}_U(x)) = \sum_{m=-NM}^{m=+NM} (w_U)_k^{(m)} e^{imax}. \quad (\text{A.1})$$

Now, it is required to determine $(w_U)_k^{(m)}$, which is presented below:

From recurrence relation it is known:

$$T_{k+1}(\hat{y}) = 2\hat{y}T_k(\hat{y}) - T_{k-1}(\hat{y}). \quad (\text{A.2})$$

Specifically, along the upper wall this relation can be written as:

$$T_{k+1}(\hat{y}_U) = 2\hat{y}_U T_k(\hat{y}_U) - T_{k-1}(\hat{y}_U). \quad (\text{A.3})$$

Combining equation (A.1) and equation (A.3), it can be written:

$$\sum_{m=-NM}^{NM} (w_U)_{k+1}^{(m)} e^{imax} = 2\hat{y}_U \sum_{m=-NM}^{NM} (w_U)_K^{(m)} e^{imax} - \sum_{m=-NM}^{NM} (w_U)_{K-1}^{(m)} e^{imax}. \quad (\text{A.4})$$

Taking Fourier expansion of \hat{y}_U :

$$\hat{y}_U = \sum_{n=-\infty}^{\infty} A_U^{(n)} e^{inax} \approx \sum_{n=-NM}^{NM} A_U^{(n)} e^{inax}. \quad (\text{A.5})$$

Combining equation (A.4) and equation (A.5):

$$\begin{aligned} \sum_{m=-NM}^{NM} (w_U)_{k+1}^{(m)} e^{imax} &= 2 \sum_{n=-NM}^{NM} A_U^{(n)} e^{inax} \sum_{m=-NM}^{NM} (w_U)_K^{(m)} e^{imax} - \\ \sum_{m=-NM}^{NM} (w_U)_{K-1}^{(m)} e^{imax}. \end{aligned} \quad (\text{A.6})$$

In the right-hand side of equation (A.6) there is a multiplication of two Fourier expansions. Here, it is shown, how they can be reduced to one Fourier expansion.

$$\begin{aligned} &2 \sum_{n=-NM}^{NM} A_U^{(n)} e^{inax} \sum_{m=-NM}^{NM} (w_U)_K^{(m)} e^{imax} \\ &= 2 \sum_{n=-NM}^{NM} \sum_{m=-NM}^{NM} A_U^{(n)} (w_U)_K^{(m)} e^{i(n+m)ax}. \end{aligned}$$

Let's define $m+n = p$ which gives $m = p - n$

$$= 2 \sum_{n=-NM}^{NM} \sum_{p=-NM-NM}^{NM+NM} A_U^{(n)} (w_U)_K^{(p-n)} e^{i(p)ax}.$$

Replacing index "p" with "m" gives:

$$= 2 \sum_{m=-2NM}^{2NM} \sum_{n=-NM}^{NM} A_U^{(n)} (w_U)_K^{(m-n)} e^{imax}.$$

With this, equation (A.6) stands:

$$\begin{aligned} \sum_{m=-NM}^{NM} (w_U)_{k+1}^{(m)} e^{imax} &= 2 \sum_{m=-2NM}^{2NM} \sum_{n=-NM}^{NM} A_U^{(n)} (w_U)_K^{(m-n)} e^{imax} - \\ \sum_{m=-NM}^{NM} (w_U)_{K-1}^{(m)} e^{imax}. \end{aligned}$$

Separating for each Fourier mode:

$$(w_U)_{k+1}^{(m)} = 2 \sum_{n=-NM}^{n=NM} A_U^{(n)} (w_U)_k^{(m-n)} - (w_U)_{k-1}^{(m)} \quad |k \geq 1|. \quad (\text{A.7})$$

This equation will give values of Fourier coefficient for which k is greater than or equal to 1, then how the initial terms i.e., terms corresponding to k less than 1 are to be determined? The following discussion is going to answer this question.

For $k = 0$:

From equation (A.1), the following can be written:

$$T_k(\hat{y}_U(x)) = \sum_{m=-NM}^{m=+NM} (w_U)_k^{(m)} e^{imax}.$$

It is known:

$$T_0(\hat{y}_U(x)) = 1. \quad (\text{A.8})$$

For $k = 0$, equation (A.1) stands:

$$T_0(\hat{y}_U(x)) = \sum_{m=-NM}^{m=+NM} (w_U)_0^{(m)} e^{imax}. \quad (\text{A.9})$$

Combining the above two equations:

$$\sum_{m=-NM}^{m=+NM} (w_U)_0^{(m)} e^{imax} = 1. \quad (\text{A.10})$$

For mode zero i.e., $m = 0$:

$$(w_U)_0^{(0)} = 1. \quad (\text{A.11})$$

Equation (A.10) and (A.11) can be true at the same time only when the following equation is true:

$$(w_U)_0^{(m)} = 0 \quad |m| \geq 1. \quad (\text{A.12})$$

For k = 1:

Recall equation (A.1):

$$T_k(\hat{y}_U(x)) = \sum_{m=-NM}^{m=+NM} (w_U)_k^{(m)} e^{imax}.$$

From the basic relation of Chebyshev Polynomials, the following can be written:

$$T_1(\hat{y}_U(x)) = \hat{y}_U(x). \quad (\text{A.13})$$

For k = 1, equation (A.1), stands:

$$T_1(\hat{y}_U(x)) = \sum_{m=-NM}^{m=+NM} (w_U)_1^{(m)} e^{imax}. \quad (\text{A.14})$$

Combining equation (A.13) and equation (A.14):

$$\hat{y}_U(x) = \sum_{m=-NM}^{m=+NM} (w_U)_1^{(m)} e^{imax}. \quad (\text{A.15})$$

According to equation (A.5), the following can be written:

$$\hat{y}_U = \sum_{m=-NM}^{m=+NM} A_U^{(m)} e^{imax}. \quad (\text{A.16})$$

Comparing equation (A.15) and equation (A.16):

$$\sum_{m=-NM}^{m=+NM} (w_U)_1^{(m)} e^{imax} = \sum_{m=-NM}^{m=+NM} A_U^{(m)} e^{imax}. \quad (\text{A.17})$$

Separating for each Fourier mode:

$$(w_U)_1^{(m)} = A_U^{(m)} \quad |m| \geq 0. \quad (\text{A.18})$$

Following is a summary of this sub-section:

$$(w_U)_0^{(0)} = 1. \quad (\text{A.11})$$

$$(w_U)_0^{(m)} = 0 \quad |m| \geq 1. \quad (\text{A.12})$$

$$(w_U)_1^{(m)} = A_U^{(m)} \quad |m| \geq 0. \quad (\text{A.18})$$

$$(w_U)_{k+1}^{(m)} = 2 \sum_{n=-NM}^{n=NM} A_U^{(n)} (w_U)_k^{(m-n)} - (w_U)_{k-1}^{(m)} \quad k \geq 1 \text{ and } |m| \geq 0. \quad (\text{A.7})$$

Evaluation of Fourier Expansion of first derivative of Chebyshev Polynomials

This sub-section will determine the Fourier expansion of the first derivative of Chebyshev polynomials along the upper wall:

Recall the recurrence relation:

$$T_{k+1}(\hat{y}) = 2\hat{y}T_k(\hat{y}) - T_{k-1}(\hat{y}).$$

Differentiating the recurrence relation with respect to \hat{y}

$$DT_{k+1}(\hat{y}) = 2T_k(\hat{y}) + 2\hat{y}DT_k(\hat{y}) - DT_{k-1}(\hat{y}). \quad (\text{A.19})$$

Along the upper wall this equation can be written as:

$$DT_{k+1}(\hat{y}_U) = 2T_k(\hat{y}_U) + 2\hat{y}_U DT_k(\hat{y}_U) - DT_{k-1}(\hat{y}_U). \quad (\text{A.20})$$

Let, the derivative of Chebyshev polynomial is given by

$$DT_k(\hat{y}_U(x)) = \sum_{m=-\infty}^{\infty} (d_U)_k^{(m)} e^{imax}. \quad (\text{A.21})$$

Drawing analogy from equation (A.21) and applying that in equation (A.20) gives:

$$\begin{aligned} \sum_{m=-\infty}^{\infty} (d_U)_{k+1}^{(m)} e^{imax} &= 2 \sum_{m=-\infty}^{\infty} (w_U)_k^{(m)} e^{imax} + \\ 2 \sum_{n=-\infty}^{\infty} A_U^{(n)} e^{inax} \sum_{m=-\infty}^{\infty} (d_U)_k^{(m)} e^{imax} &- \sum_{m=-\infty}^{\infty} (d_U)_{k-1}^{(m)} e^{imax}. \end{aligned} \quad (\text{A.22})$$

Performing the multiplication of two Fourier expansions in equation (A.22) can be written as:

$$2 \sum_{n=-\infty}^{\infty} A_U^{(n)} e^{inax} \sum_{m=-\infty}^{\infty} (d_U)_k^{(m)} e^{imax} = 2 \sum_{m=-\infty}^{\infty} \sum_{n=-\infty}^{\infty} A_U^{(n)} (d_U)_k^{(m-n)} e^{imax}. \quad (\text{A.23})$$

Combining equation (A.22) and (A.23):

$$\begin{aligned} \sum_{m=-\infty}^{\infty} (d_U)_{k+1}^{(m)} e^{imax} &= 2 \sum_{m=-\infty}^{\infty} (w_U)_k^{(m)} e^{imax} + \\ 2 \sum_{m=-\infty}^{\infty} \sum_{n=-\infty}^{\infty} A_U^{(n)} (d_U)_k^{(m-n)} e^{imax} &- \sum_{m=-\infty}^{\infty} (d_U)_{k-1}^{(m)} e^{imax} \\ \sum_{m=-\infty}^{\infty} (d_U)_{k+1}^{(m)} e^{imax} &= \sum_{m=-\infty}^{\infty} \left\{ 2 (w_U)_k^{(m)} + 2 \sum_{n=-\infty}^{\infty} A_U^{(n)} (d_U)_k^{(m-n)} - \right. \\ \left. (d_U)_{k-1}^{(m)} \right\} e^{imax}. \end{aligned} \quad (\text{A.24})$$

Separating for each Fourier mode above equation can be written as:

$$(d_U)_{k+1}^{(m)} = 2 (w_U)_k^{(m)} + 2 \sum_{n=-\infty}^{\infty} A_U^{(n)} (d_U)_k^{(m-n)} - (d_U)_{k-1}^{(m)}. \quad (\text{A.25})$$

Appendix B: Evaluation of Innerproducts of Chebyshev polynomials and their derivatives

This section will describe the evaluation of the Innerproducts of Chebyshev polynomials and their derivatives. Definition of the inner product of two Chebyshev polynomials can be given by as follows

$$\langle T_j(\hat{y}), T_k(\hat{y}) \rangle_{\omega} = \int_{-1}^1 T_j(\hat{y}) T_k(\hat{y}) \omega(\hat{y}) d\hat{y}, \quad \omega(\hat{y}) = \sqrt{1 - \hat{y}^2}, \quad (\text{B.1})$$

here ω is the weight function.

By orthogonality properties of Chebyshev Polynomials, simple solutions for the above integral can be presented as

$$\begin{aligned} \langle T_j, T_k \rangle &= \frac{\pi}{2} C_k \delta_{j,k} = \pi, \quad j = k = 0 \\ &= \frac{\pi}{2}, \quad j = k \geq 1 \\ &= 0, \quad j \neq k \end{aligned} \quad (\text{B.2})$$

where $\delta_{j,k}$ is the Kroneckerdelta and C_k is defined as

$$\begin{aligned} C_k &= 2, \quad k = 0 \\ &= 1, \quad k \geq 1 \end{aligned} \quad (\text{B.3})$$

Chebyshev polynomials can be used to express the first derivative of Chebyshev polynomial as follows:

$$DT_k = 2k \sum_{x=0}^{k-1} \frac{1}{c_x} T_x, \quad k - x = \text{odd}, \quad k \geq x + 1 \quad (\text{B.4})$$

Taking the inner product of this derivative with Chebyshev polynomial T_j gives

$$\langle T_j, DT_k \rangle = 2k \sum_{x=0}^{k-1} \frac{1}{c_x} \langle T_j, T_x \rangle, \quad k - x = \text{odd}, \quad k \geq x + 1$$

By inserting (B.2) in the above equation the relation for inner product of a Chebyshev polynomial of j -th order and its first derivative of k -th order can be obtained as follows

$$\langle T_j, DT_k \rangle = k\pi, \quad k - j = \text{odd}, \quad k \geq j + 1 \quad (\text{B.5})$$

The expression for the second derivative of a Chebyshev polynomial is given by

$$D^2T_k = \sum_{x=0}^{k-2} \frac{1}{c_x} k(k^2 - x^2)T_x, \quad k - x = \text{even}, \quad k \geq x + 2 \quad (\text{B.6})$$

Multiplying (B.6) by Chebyshev polynomial T_j and integrating between -1 and +1 results in

$$\langle T_j, D^2T_k \rangle = \sum_{x=0}^{k-2} \frac{1}{c_x} k(k^2 - x^2) \langle T_j, T_x \rangle, \quad k - x = \text{even}, \quad k \geq x + 2$$

By substituting (B.2) in the above equation a suitable relation for inner product of a Chebyshev polynomial of j -th order and its second derivative of k -th order is obtained as follows

$$\langle T_j, D^2T_k \rangle = k(k^2 - j^2) \frac{\pi}{2}, \quad k - j = \text{even}, \quad k \geq j + 2 \quad (\text{B.7})$$

By differentiating (B.6) with respect to \hat{y} a similar relation for the third derivative of Chebyshev polynomial can be obtained as:

$$D^3T_k = D(D^2T_k) = \sum_{x=0}^{k-2} \frac{1}{c_x} k(k^2 - x^2)DT_x, \quad k - x = \text{even}, k \geq x + 2$$

Substituting (B.4) in the above equation, the following equation for the third derivative of a Chebyshev polynomial can be obtained

$$D^3T_k = \sum_{x=0}^{k-2} \frac{1}{c_x} k(k^2 - x^2) \left[2x \sum_{z=0}^{x-1} \frac{1}{c_z} T_z \right] \quad (\text{B.8})$$

where, $k - x = \text{even}, k \geq x + 2$; $x - z = \text{odd}, x \geq z + 1$

Taking the inner product of (B.8) with T_j and using (B.2), a suitable relation for inner product of a Chebyshev polynomial of j -th order and its third derivative of k -th order can be obtained as follows:

$$\langle T_j, D^3T_k \rangle = \sum_{x=0}^{k-2} \frac{1}{c_x} k(k^2 - x^2)(\pi x) \quad (\text{B.9})$$

$k - x = \text{even}, k \geq x + 2$; $x - j = \text{odd}, \text{ and } x \geq j + 1$

By differentiating (B.6) twice, the fourth derivative of Chebyshev polynomial is obtained as follows:

$$D^4T_k = D^2(D^2T_k) = \sum_{x=0}^{k-2} \frac{1}{c_x} k(k^2 - x^2)D^2T_x, \quad k - x = \text{even}, k \geq x + 2$$

By using (B.6) for D^2T_x in the above equation a relation for the fourth derivative of a Chebyshev polynomial is obtained as follows

$$D^4T_k = \frac{d^2}{dy^2} (D^2T_k) = \sum_{x=0}^{k-2} \frac{1}{c_x} k(k^2 - x^2) \left[\sum_{z=0}^{x-2} \frac{1}{c_z} x(x^2 - z^2)T_z \right] \quad (\text{B.10})$$

$k - x = \text{even}, k \geq x + 2$; $x - z = \text{even}, x \geq z + 2$

By taking the inner product of Chebyshev polynomial with this function the following is obtained

$$\langle T_j, D^4 T_k \rangle = \sum_{x=0}^{k-2} \frac{1}{C_x} k(k^2 - x^2) \left[x(x^2 - j^2) \frac{\pi}{2} \right] \quad (\text{B.11})$$

$$k - x = \text{even}, \quad k \geq x + 2 \geq j + 4 \quad ; \quad x - j = \text{even}, x \geq j + 2$$

Curriculum Vitae

Name: Kh Md Faisal

Post-secondary Education and Degrees: Military Institute of Science and Technology
Mirpur Cantonment, Dhaka Bangladesh
2009-2012 B.Sc. in Aeronautical Engineering
(major in Aerospace)

Military Institute of Science and Technology
Mirpur Cantonment, Dhaka Bangladesh
2014-2017 (part-time) M.Sc. in Mechanical Engineering

The University of Western Ontario
London, Ontario, Canada
2018-2020 M.E.Sc. in Mechanical Engineering

Honors and Awards: Western Graduate Research Scholarship
2018-2020
GTA Research Contribution Award- Scholarship
2019

Related Work Experience Teaching and Research Assistant
The University of Western Ontario
2018-2020